

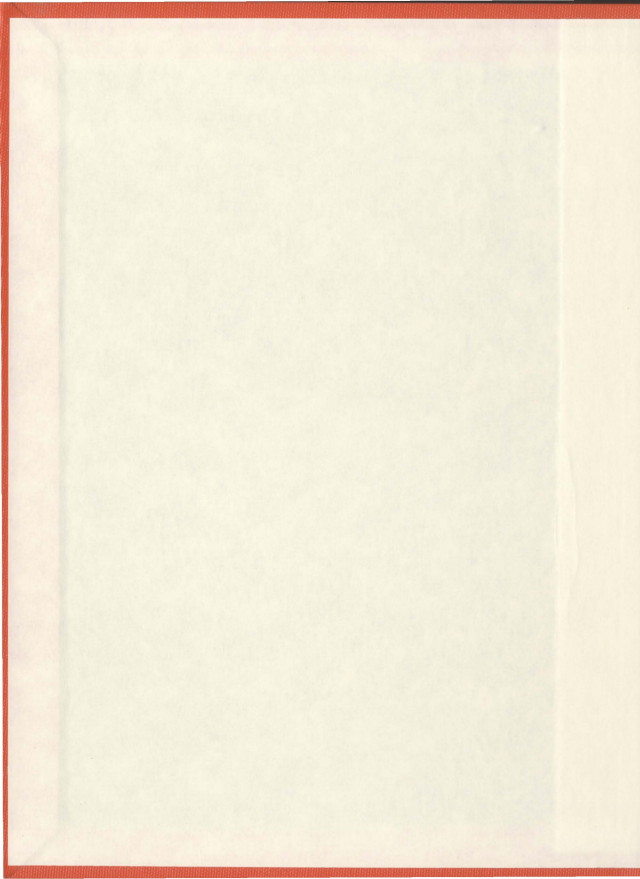
A STUDY OF A NOVEL MEMBRANE-BASED
LIQUID-GAS CONTACTOR

CENTRE FOR NEWFOUNDLAND STUDIES

**TOTAL OF 10 PAGES ONLY
MAY BE XEROXED**

(Without Author's Permission)

SHUNYU WANG



A STUDY OF A NOVEL MEMBRANE-BASED LIQUID-GAS CONTACTOR

by

© Shunyu Wang

A thesis submitted to the
School of Graduate Studies
in partial fulfilment of the
requirement for the degree of
Master of Engineering

Faculty of Engineering and Applied Science
Memorial University of Newfoundland

August 2005

St. John's



Newfoundland

Abstract

Two dual-membrane configurations were conceptually proposed to improve the performance of the ordinary single-membrane contactor. In Configuration 1, a second porous membrane was added and a flow of sweeping gas was introduced on the permeate side of the second membrane; in Configuration 2, the second membrane was a nonporous one, and a low pressure was applied on the permeate side of the nonporous membrane. Theoretically both configurations can partially regenerate the solvent stream simultaneously with the absorption process. Since the rate of acid gas absorption is a function of the concentration of acid components in the solvent, by continuous removal of these components from the solvent, a better absorption efficiency can be obtained. The new ideas were first simulated using partial differential equations and corresponding initial and boundary conditions based on one-component absorption, and the Crank-Nicholson method was used to obtain the numerical solutions. The solutions showed that the novel dual-membrane contactors can remove acid components more efficiently than the ordinary membrane contactor. Based on a single-component absorption simulation, analyses were carried out to examine the effects of a variety of parameters on the removal efficiency. In addition, the mathematic model for multi-component system in which more than one component participated in absorption was developed and solved to simulate acid gas removal in natural gas handling.

Acknowledgements

I would like to express my sincere gratitude to my supervisors Dr. Majid A. Abdi and Dr. Kelly Hawboldt for their enthusiastic guidance, supervision and encouragement during the period of my study. The experience of working with them has been more than rewarding.

I would also give my appreciation to:

1. School of Graduate Studies, Memorial University of Newfoundland (MUN) for the financial support;
2. Professors in the Faculty of Engineering for the courses they offered;
3. My wife and my parents for their spiritual support;
4. Ms. Janet Bengier and her assistants in ESL (English as a Second Language) program for improving my academic English skills;
5. Fellow graduate students in Faculty of Engineering who made me feel at home during the past two years.

Table of Contents

Abstract.....	i
Acknowledgements	ii
Table of Contents	iii
List of Figures.....	vi
List of Tables	vi
Nomenclature	x
Chapter 1 Introduction.....	1
1.1 Background	1
1.2 Scope of Study	2
1.3 Objectives of Study.....	4
1.4 Thesis Outline	6
Chapter 2 Introduction to Membrane Contactors	7
2.1 Introduction to Membrane Technology	7
2.1.1 Porous Membrane and Nonporous Membrane	7
2.1.2 Membrane Processes.....	8
2.1.3 Membrane Modules	9
2.2 Transport in Membranes	11
2.2.1 Transport through Porous Membranes.....	11
2.2.2 Nonporous Membrane	13
2.3 Membrane Contactors.....	15
2.3.1 Wetted and Nonwetted Mode	15
2.3.2 Overall Mass Transfer Coefficient.....	17
Chapter 3 Mathematical Models	19
3.1 Relevant Fluid Dynamics and Mass Transfer Fundamentals	19
3.1.1 Fully Developed Laminar Flow	19

3.1.2 Diffusion Mass Transfer	21
3.1.3 Convective Mass Transfer	21
3.1.4 Governing Mass Transfer Equation	22
3.2 Model Development:	23
3.2.1 Configuration 1	24
3.2.2 Configuration 2	26
3.2.3 Ordinary Membrane Contactor	28
Chapter 4 Solutions to Model Equations	31
4.1 Numerical Solution	32
4.1.1 Application of the Crank-Nicholson Method	32
4.1.2 Configuration 1	37
4.1.3 Configuration 2	40
4.1.4 Ordinary Membrane Contactor	42
4.1.5 Comparison and Analysis	44
4.2 Bulk Concentration Method.....	46
4.2.1 Modeling in Bulk Concentration Method	49
4.2.2 Comparison of Three Configurations	54
4.3 Analytical Solution	57
4.3.1 Numerical Solution to Simplified Model.....	59
4.3.2 Analytical Solution (Asymptotic solution)	60
4.3.3 Comparison between Numerical and Analytical Solutions	64
Chapter 5 Impact of Model Parameters on Performance.....	66
5.1 Channel Height	66
5.2 Permeate Side Pressure	68
5.3 The Henry's Constant	69
5.4 Diffusivity	71
5.5 Solvent Flow Rate.....	72
5.6 Permeability	73
5.7 Mixture Gas Pressure	75

Chapter 6 Multi-component System	78
6.1 Mathematical Model	78
6.2 Numerical Solution	82
Chapter 7 Conclusions.....	89
7.1 Summary	89
7.2 Conclusion	90
7.3 Follow-up work.....	91
References	92
Appendix A The Properties of H₂S and CO₂ in Methanol.....	94
Appendix B Crank-Nicholson Technique.....	97
Appendix C Matlab and Maple Code	102

List of Figures

Figure 1. 1 Schematic drawing of an ordinary single-membrane contactor	3
Figure 1. 2 Schematic drawing of Configuration 1	4
Figure 1. 3 Schematic drawing of Configuration 2.....	4
Figure 2. 1 Schematic drawing of a plate-and-frame module.....	10
Figure 2. 2 Schematic drawing of a spiral-wound module	10
Figure 2. 3 Schematic drawing of a hollow fibre module.....	10
Figure 2. 4 Schematic drawings of Poiseuille and Knudsen flows	11
Figure 2. 5 Nonwetted mode of membrane-based gas-liquid contacting	16
Figure 2. 6 Wetted mode of membrane-based gas-liquid contacting	17
Figure 2. 7 Mass transfer regions in a membrane contactor	18
Figure 3. 1 Velocity profile for fully developed laminar flow between infinite parallel plates	20
Figure 3. 2 Schematic arrangement of membranes in Configuration 1	24
Figure 3. 3 Schematic arrangement of membranes in Configuration 2	26
Figure 3. 4 Schematic drawing of ordinary membrane contactor.....	28
Figure 4. 1 Grid on solvent domain	33
Figure 4. 2 CO ₂ concentration profiles under co-current flow conditions for Configuration 1	39
Figure 4. 3 CO ₂ concentration profiles under counter current flow conditions for Configuration 1	39
Figure 4. 4 CO ₂ concentration profiles under co-current flow conditions for Configuration 2	41
Figure 4. 5 CO ₂ concentration profiles under counter current flow conditions for Configuration 2	41

Figure 4. 6 CO ₂ concentration profiles under co-current flow conditions for ordinary membrane contactor.....	43
Figure 4. 7 CO ₂ concentration profiles under counter current flow conditions for the ordinary membrane contactor	43
Figure 4. 8 CO ₂ concentration profiles in mixture gas under counter current flow conditions.....	44
Figure 4. 9 CO ₂ concentration profiles in solvent under counter current flow conditions	45
Figure 4. 10 Schematic drawing of component <i>i</i> transfer through nonporous membrane	47
Figure 4. 11 Bulk modeling schematic drawing for Configuration 1	49
Figure 4. 12 CO ₂ concentration profiles under counter current flow conditions for Configuration 1 based on “bulk concentration ” approach.....	51
Figure 4. 13 Bulk modeling schematic drawing for Configuration 2	51
Figure 4. 14 CO ₂ concentration profiles under counter current flow conditions for configuration 2 based on “bulk concentration” approach.....	52
Figure 4. 15 Bulk modeling schematic drawing for ordinary membrane contactor	53
Figure 4. 16 CO ₂ concentration profiles under counter current flow conditions for ordinary membrane contactor based on “bulk concentration ” approach	54
Figure 4. 17 CO ₂ concentration profiles in mixture gas under counter current flow conditions based on “bulk concentration ” approach.....	55
Figure 4. 18 CO ₂ concentration profiles under counter current flow conditions for Configuration 1	56
Figure 4. 19 CO ₂ concentration profiles under counter current flow conditions for Configuration 2	56
Figure 4. 20 CO ₂ concentration profiles under counter current flow conditions for ordinary membrane contactor	57
Figure 4. 21 Simplified membrane contactor	58
Figure 4. 22 CO ₂ concentration in solvent profile from numerical solution	59
Figure 4. 23 CO ₂ concentration in solvent profile from analytical solution	64

Figure 4. 24 CO ₂ concentration in solvent profiles from analytical and numerical solutions	65
Figure 5. 1 The effect of channel height on acid gas removal	67
Figure 5. 2 The effect of permeate side pressure on acid gas removal	68
Figure 5. 3 The effect of Henry's constant on acid gas removal	70
Figure 5. 4 The effect of diffusivity on acid gas removal.....	71
Figure 5. 5 The effect of solvent flow rate on acid gas removal.....	72
Figure 5. 6 The effect of permeability on acid gas removal	74
Figure 5. 7 The effect of permeability on acid gas removal	74
Figure 5. 8 The effect of mixture gas pressure on acid gas removal	76
Figure 6. 1 Schematic drawing of multi-component absorption.....	79
Figure 6. 2 CO ₂ and H ₂ S concentration profiles for multi-component system.....	85
Figure 6. 3 CO ₂ and H ₂ S concentration in mixture gas profiles for dual-membrane and single-membrane contactors ($P_{out} = 2.0 \times 10^5$ PaA).....	87
Figure 6. 4 CO ₂ and H ₂ S concentration profiles from dual-membrane and single-membrane contactors ($P_{out} = 0$).....	88
Figure B. 1 Grid on time-space domain.....	98
Figure B. 2 Crank-Nicholson method.....	98

List of Tables

Table 2. 1 Classification of membrane processes according to their driving forces.....	8
Table 2. 2 The permeability of carbon dioxide and methane in various polymers	14
Table 4. 1 Parameters used in calculations	37
Table 4. 2 CO ₂ inlet and outlet concentration for Configuration 1	38
Table 4. 3 CO ₂ inlet and outlet concentration for Configuration 2	40
Table 4. 4 CO ₂ inlet and outlet concentration for ordinary membrane contactor	42
Table 4. 5 Parameters used in calculations	59
Table 6. 1 Parameters used in calculations for multi-component system	84
Table 6. 2 Outlet CO ₂ and H ₂ S concentrations for multi-component system for the dual- membrane contactor ($P_{out} = 2.0 \times 10^5$ PaA).....	86
Table 6. 3 Outlet CO ₂ and H ₂ S concentrations in mixture gas for dual-membrane and single-membrane contactors ($P_{out} = 2.0 \times 10^5$ PaA).....	86

Nomenclature

A	Cross area of liquid flow, m^2
C	Mole concentration, $kgmol/m^3$
\bar{C}	Average mole concentration, $kgmol/m^3$
D	Diffusion coefficient, m^2/s
D_k	Knudsen diffusion coefficient
H	Henry's constant
h	Height of channel, m
J	Mole flux, $kgmol/s$
K	Overall mass transfer coefficient, m/s
k_g, k_m, k_l	Mass transfer coefficient in gas, membrane and liquid, respectively, m/s
L	Length of membrane, m
M_w	Molecular weight
N_g	Mole flow rate of gas, $kgmol/s$
P	Pressure, Pa
Per	Permeability coefficient, Barrer
Q	Volumetric flow rate, m^3/s
R	Gas constant, $m^3Pa/kgmolK$
r	Pore radius, m
S	Area of membrane, m^2

Sol	Solubility coefficient in membrane, $m^3(STP)/m^3Pa$
T	Temperature, K
u	Velocity, m/s
w	Width of membrane, m
x	Length coordinate position, m
y	Height coordinate position, m
z	Gas mole percentage, %

Greek symbols

δ	Thickness of membrane, m
μ	Viscosity, Ns/m^2
ρ	Density, kg/m^3
τ	Pore tortuosity

Subscripts

A	Component A
B	Component B
g	Gas phase
l	Liquid phase

Chapter 1

Introduction

1.1 Background

During the past 30 years, solvent absorption dominated the natural gas treatment (including CO₂, H₂S removal, dehydration, etc.) field, where the solvent can be various amine, formulated mixed or glycol solutions depending on the purpose of the treatment. The absorption process can be physical or chemical or a combination of the two. The applications of membrane technology in natural gas engineering consist of two different branches: membrane gas separation and membrane gas absorption. The former is a pressure-driven process in which no gas-liquid contact happens and the selectivity of the membrane determines the efficiency of the separation. Membrane gas absorption devices (also called membrane contactors) are the focus of this thesis, in which the membrane does not function as a species selective barrier, but rather a material supplying the interfacial area for gas-liquid mass transfer.

Membrane gas absorption shows a very promising potential in providing an alternative to the traditional absorption processes. This process bears a number of advantages over traditional gas-liquid absorption [1]:

1. The membrane modules are small and light, making it ideally suitable for offshore applications;

2. There are no operational limitations like flooding, loading, weeping, etc, which result in much less need for human supervision and maintenance compared to conventional gas-liquid contactors;
3. The density difference of the contacting phases is irrelative to membrane contactors. Hence, the orientations of the contactor and the sway have little impact to the performance, which makes it ideal for offshore and floating production and/or processing applications;
4. Membrane system can supply a much larger interfacial area per unit volume than conventional contactors;
5. The scale-up of the membrane system is linear to its modular number, so the treatment capacities can be easily adjusted according to the production.

1.2 Scope of Study

This thesis will focus on membrane-based physical gas absorption and techniques to improve the performance of this process. The membrane contactor is a combination of membrane and conventional physical absorption technology, so that the advantages of membrane as well as the good performance of absorption can be utilized. Usually porous membranes are used in membrane contactors. By a suitable choice of membrane and operating conditions, the phase boundary can be kept stabilized at the pore mouth of the membrane. This configuration provides a dispersionless gas-liquid contact in which the interfacial area for mass transfer is the membrane surface area. Figure 1.1 illustrates the mechanism for ordinary membrane contactor [1].

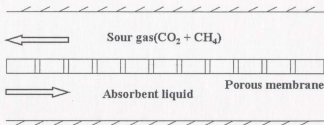


Figure 1. 1 Schematic drawing of an ordinary single-membrane contactor

Acid gas removal is one of the most common gas processing requirements in gas industry, so this thesis will focus on the study of novel membrane contactors in sour gas treatment. This research proposes two novel configurations to improve the performance of the ordinary single-membrane contactor. In Configuration 1, a second porous membrane is added and a flow of sweeping gas is introduced on the permeate side of the second membrane (See Figure 1.2). In Configuration 2, the second membrane is a nonporous one, and a low pressure (slightly higher than atmosphere pressure) is applied on the permeate side of the nonporous membrane (See Figure 1.3). The sweeping gas in Configuration 1 or the differential pressure across the nonporous membrane in Configuration 2 can partially strip the acid gas components from the solvent, thereby partially regenerating the solvent stream simultaneously with the absorption process. Since the rate of acid gas absorption is a function of the concentration of acid gas components in the liquid phase, by continuous removal of these components from the solvent, better absorption efficiency can be obtained.

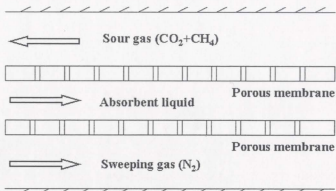


Figure 1. 2 Schematic drawing of Configuration 1

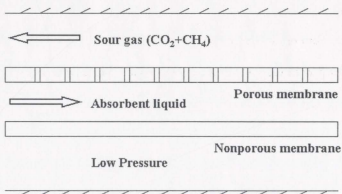


Figure 1. 3 Schematic drawing of Configuration 2

1.3 Objectives of Study

The purpose of this research is to conceptualize a regenerative absorption system by using a dual-membrane system. First of all, we proposed two configurations to improve the performance of an ordinary single-membrane contactor. Then, to demonstrate the novel dual-membrane systems can give an improved performance as expected, we mathematically modeled them and compared them with the ordinary single-membrane

contactor based on the modeling results. Partial differential equations were used to model the dual-membrane contactors and the ordinary membrane contactor, and numerical method was used to solve them. To understand the effects of various parameters on the separation performance, operating parameters were changed independently in a step-by-step procedure. In addition, based on single-component absorption, a modeling methodology for multi-component absorption is developed to simulate sour gas treatment in natural gas industry.

Due to the fact that this research only aims at proving the concepts and also the high-pressure requirement for experimental performance studies, the model was not verified experimentally at this point. However, to make sure the modeling and the numerical solutions are accurate, the process was also modeled with "bulk concentration" approach, in which mass transfer coefficients in the liquid phase was introduced. Because the mass transfer coefficient is an empirical correlation, the "bulk concentration" method did not show the exactly same solutions as the partial differential model, but it did show the same trend. This can further demonstrate conceptually that the new dual-membrane contactor can improve the separation performance. In addition, in an attempt to check the numerical solution analytically, the boundary conditions of the model were simplified to make the analytical solution available. The analytical solution to the model with simplified boundary conditions proved the Matlab code concerning partial differential equation part was correct.

1.4 Thesis Outline

This thesis is divided into seven chapters. Chapter 1 presents a preliminary introduction to the thesis, and gives the concept of membrane contactor and what is new about this research. In Chapter 2, the fundamentals concerning membrane technology, transport mechanism through membranes and the membrane contactor are presented to give readers a basic understanding of membrane contactor. In Chapter 3, partial differential equations and corresponding initial and boundary conditions are developed to simulate the proposed dual-membrane contactors (including Configuration 1 and Configuration 2) and the ordinary membrane contactor based on single-component absorption. In Chapter 4, the models are numerically solved using the Crank-Nicholson method. Comparisons between the novel dual-membrane contactors and the single-membrane contactor are carried out. Then Configuration 2 is recommended based on industrial consideration. In addition, the accuracy of numerical solution for Configuration 2 is verified by a "bulk concentration" approach as well as an asymptotic solution in this chapter. In Chapter 5, according to the modeling results, analysis is implemented to check the effect on the performance of various operating parameters. In Chapter 6, based on single-component absorption modeling, a methodology is described for multi-component absorption, and a two-component absorption process is utilized to present the methodology. In Chapter 7, summary and conclusions of this thesis as well as some suggestions for future work are presented.

Chapter 2

Introduction to Membrane Contactors

This chapter presents a brief introduction to membrane technology, including the definition of porous and nonporous membranes, membrane processes and membrane modules. Then mechanisms of gas molecule diffusing through porous and nonporous membranes are also explained. The fundamentals of the ordinary single-membrane contactor used in natural gas industry are subsequently described.

2.1 Introduction to Membrane Technology

2.1.1 Porous Membrane and Nonporous Membrane

Membranes are physical media providing the means for the separation of the components in a mixture. Membranes can be made from various polymers, as well as ceramics, carbon fibre, and so on. According to the pore size, membranes can be categorized into two types, namely porous and nonporous membranes. International Union of Pure and Applied Chemistry (IUPAC) classifies the pores in membranes in terms of the pore size as follows [2]:

Macropores: pore size >50 nm

Mesopores: $2\text{nm} < \text{pore size} < 50$ nm

Micropores: pore size $< 2\text{nm}$

Here the pore size is referred to the pore diameter or more arbitrarily the pore width. Membranes with macropores or mesopores are classified into the porous membrane

category. For porous membranes, the pore size and its distribution determine which particles or molecules are retained and which can pass through the membrane, so it is the pore characteristic not material that determines the separation performance. Membranes without fixed pores are nonporous membrane. For nonporous membranes, such as pervaporation and gas separation membranes, the material itself determines the separation performance.

2.1.2 Membrane Processes

In all membrane processes, components being separated diffuse through the membrane when a driving force is applied. The driving force can be pressure difference, concentration difference, temperature difference or electrical potential difference across the membrane. The membrane processes can be classified based on the difference in the driving force as shown in Table 2.1 [2].

Table 2. 1 Classification of membrane processes according to their driving forces

Pressure difference	Concentration difference	Temperature difference	Electrical potential difference
Microfiltration	Pervaporation	Thermo-osmosis	Electrodialysis
Ultrafiltration	Gas separation	Membrane-	Electro-osmosis
Nanofiltration	Membrane gas	distillation	Membrane
Reverse osmosis	absorption		electrolysis
	Vapour permeation		
	Dialysis		
	Diffusion dialysis		
	Carrier mediated		

Currently, not all the membrane processes can be applied commercially. In the pressure difference category, microfiltration, ultrafiltration and nanofiltration applications are common in the water treatment and food industries (e.g. desalination of seawater using reverse osmosis). In the concentration difference category, pervaporation is the only process with phase change, and the related application can be found in chemical process industry, food and pharmaceutical industries. Membrane gas separation and membrane gas absorption are very promising techniques in natural gas treatment, the latter being the focus of this thesis. There are few applications commercialized with temperature difference or electrical potential difference as the driving force.

2.1.3 Membrane Modules

A number of membrane module designs are available, out of which the plate-and-frame, hollow fibre, and spiral-wound modules are the most common. Generally, a particular membrane application consists of a number of modules arranged in a certain configuration. The choice and the arrangement of the modules are based on: the type of separation problem, ease of cleaning, ease of maintenance, ease of operation, compactness of the system, scale and the possibility of membrane replacement, etc. Figure 2.1, 2.2, and 2.3 show schematic drawings of plate-and-frame, hollow fibre, and spiral-wound modules, respectively [2].

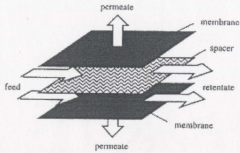


Figure 2. 1 Schematic drawing of a plate-and-frame module

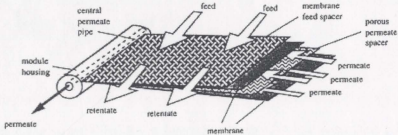


Figure 2. 2 Schematic drawing of a spiral-wound module

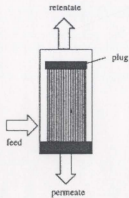


Figure 2. 3 Schematic drawing of a hollow fibre module

2.2 Transport in Membranes

As mentioned above, membranes can be classified into two groups, porous and nonporous. The transport mechanisms of gas molecules through these two types of membranes are completely different.

2.2.1 Transport through Porous Membranes

When gas molecules diffuse through porous membranes, two main flows, Knudsen flow and Poiseuille flow (viscous flow) may contribute to the total flow; which one will dominate is mainly dependent on the pore size. When the pore size is large enough ($r > 10\mu m$), Poiseuille flow occurs. In this mechanism, because the mean free path of gas molecules is very small compared to the pore diameter, the gas molecules collide with each other rather than the membrane and therefore no separation is achieved between various gas components. By decreasing the diameter of the pores, the mean free path of gas molecules becomes comparable or larger than the pore diameter. Then collisions between the gas molecules are less frequent than collisions with the pore wall. This is called Knudsen diffusion. Figure 2.4 shows the schematic drawings of the Poiseuille and Knudsen flows.

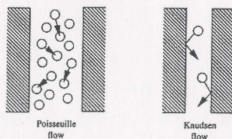


Figure 2. 4 Schematic drawings of Poiseuille and Knudsen flows

The average distance traversed by gas molecule between collisions is the mean free path. The mean free path is proportional to the temperature and inversely proportional to the pressure. Generally, the pore diameter of porous membranes is much smaller than the mean free path of gas molecular at low pressures. Therefore, at low pressure, transport of gases through porous membrane is determined mainly by Knudsen flow which can be expressed by the equation:

$$J = \frac{\pi n r^2 D_k \Delta P}{RT \tau \delta} \quad (2.1)$$

where J is the flux of the gas component; T is the temperature; r is the pore radius; δ is the thickness of the membrane; R is gas constant; ΔP is the pressure difference across membrane, n is the number of pores; τ is the pore tortuosity; D_k is the Knudsen diffusion coefficient, given by:

$$D_k = 0.66r \sqrt{\frac{8RT}{\pi M_w}} \quad (2.2)$$

where T and M_w are the temperature and molecular weight respectively and r is the pore radius. This equation shows that the flux is inversely proportional to the square root of the molecular weight and for a given membrane and pressure difference, molecular weight of the gas is the only parameter which determines the flux. Hence, the separation of two gases by Knudsen flow mechanism depends on the ratio of the square root of their corresponding molecular weights. This means the separation factor achieved by Knudsen flow mechanism is very low, so porous membrane is not a good choice in gas separation [2]. In natural gas industry, porous membranes are often used in membrane gas absorption, which will be discussed later.

2.2.2 Nonporous Membrane

A variety of nonporous membranes are used extensively in gas separation. Gas separation through nonporous membranes mainly depends on the difference in the permeability of various gas components through the membrane. Under steady-state conditions, gas permeation through a nonporous membrane is generally described by the following equation [2]:

$$J_i = \frac{D_i Sol_i (P_{o,i} - P_{t,i})}{\delta} \quad (2.3)$$

where Sol_i is the solubility coefficient of component i in the membrane; D_i is the diffusion coefficient; $P_{o,i}$ and $P_{t,i}$ stand for the partial pressure of component i on the upstream and downstream sides of the membrane respectively; δ is the thickness of the membrane.

The product of the diffusion coefficient D_i and the solubility coefficient S_i is called the permeability coefficient Per_i (i.e. $Per_i = D_i S_i$). Thereby gas permeation equation can be written as:

$$J_i = \frac{Per_i (P_{o,i} - P_{t,i})}{\delta} = \frac{Per_i}{\delta} \cdot \Delta P_i \quad (2.4)$$

This equation shows that the flux across a nonporous membrane is proportional to the partial pressure difference and inversely proportional to the membrane thickness. The ratio of the permeability coefficients of different gases is called ideal selectivity. However, the real selectivity is not equal to the ideal selectivity for a multi-component system at high pressures due to the plasticisation. High permeability contributes to a high

flux; meanwhile high selectivity gives a good separation factor; hence, membranes (generally composite membrane) with both high permeability and high selectivity are preferred.

The permeability coefficients of gases through various membranes can be collected from simple permeation experiment based on the gas permeation equation. Table 2.2 lists the permeability of carbon dioxide and the ideal selectivity of carbon dioxide and methane for various membranes.

Table 2.2 The permeability of carbon dioxide and methane in various polymers

Polymer	Per_{CO_2} (Barrer [*])	Per_{CO_2} / Per_{CH_4}
Polytrimethylsilylpropyne	33100	2.0
Silicone rubber	3200	3.4
Natural rubber	130	4.6
Polystyrene	11	8.5
Polyamide (Nylon)	0.16	11.2
Poly (vinyl chloride)	0.16	15.1
Polycarbonate (Lexan)	10.0	26.7
Polysulfone	4.4	30.0
Polyethyleneterephthalate (Mylar)	0.14	31.6
Cellulose acetate	6.0	31.0
Poly (ether imide) (Ultem)	1.5	45.0

* 1 Barrer = $0.76 \cdot 10^{-17} \text{ m}^3 \text{ (STP) m}^{-2} \text{ s}^{-1} \text{ Pa}^{-1}$

2.3 Membrane Contactors

Unlike membrane separation, where the separation depends on the selectivity of the membrane, the separation in membrane contactors depends on the difference in solubilities of various components of the gas mixture in the absorbent liquid. It is not the enhanced mass transfer coefficient but the larger interfacial area membranes can provide that makes membrane contactors work more efficiently compared to traditional gas absorption processes. For instance, packed and trayed columns can supply an interfacial area around 30-300 m^2/m^3 , whereas membrane contactors can provide a surface area of 1600-6600 m^2/m^3 . Thereby membrane contactors can reduce the volume of equipment required for gas absorption by more than 20 times, which is essentially preferable for offshore applications where the footprint area and space are at premium. The other advantages of membrane contactors are already mentioned in Chapter 1. However, membrane contactors have some potential disadvantages as well. The first one is that the total mass transfer resistance may potentially increase due to the introduction of the membrane; this problem will be discussed later [2]. Hollow fibre membrane contactor is the most popular research topic; however, this thesis will deal with the plat-and-frame membrane contactors for simplicity.

2.3.1 Wetted and Nonwetted Mode

In general, porous membranes are used in membrane contactors. The porous membrane functions as a fixed barrier between the gas and the liquid absorbent while gas components diffuse through the membrane, thereby keeping gas and liquid from dispersing into each other. Membrane materials can be hydrophobic or hydrophilic. The

pores of the membrane can be filled with either gas or liquid depending on membrane material, the physicochemical properties of the absorbent liquid, and the operating pressures employed [3].

When a hydrophobic membrane is used with an aqueous solvent, the membrane is under the nonwetted mode, i.e. the pores are filled with gases and the liquid does not wet the membrane. Under this mode, the liquid phase pressure should be higher than gas pressure to prevent gas dispersing into liquid as bubbles and lower than wetting pressure to prevent the wetting of the membrane. The gas-liquid interface lies at the pore mouth of the membrane on the absorbent liquid side. Figure 2.5 gives a schematic description of this mode [4].

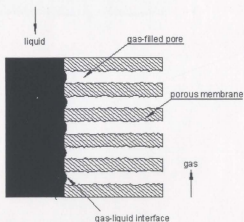


Figure 2. 5 Nonwetted mode of membrane-based gas-liquid contacting

When hydrophilic membranes are used with aqueous absorbents, liquid will wet the membrane spontaneously, i.e. the pores are filled with liquid. Figure 2.6 explains this mode schematically. Under this mode, gas pressure has to be higher than liquid phase

pressure to prevent liquid from dispersing as drops into gas. This mode is preferred when the mass transfer is controlled by gas phase. For instance, a very fast or instantaneous chemical reaction occurs between the gas component and the solvent liquid, or the gas solubility in the liquid is very high [4].

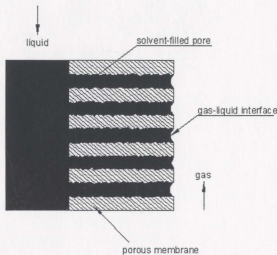


Figure 2. 6 Wetted mode of membrane-based gas-liquid contacting

2.3.2 Overall Mass Transfer Coefficient

In natural gas industry, gas absorption can be physical or chemical; only physical absorption is discussed in this thesis. Membrane-based physical absorption is generally operated under nonwetted mode. The transfer of gas molecules from gas phase to the liquid consists of three steps shown in Figure 2.7: transfer from bulk of the gas phase to membrane, diffusion through the gas-filled pores, and transfer from membrane into bulk of the liquid phase. The flux can be expressed in the following expression:

$$J_i = K_i \Delta C_i \quad (2.5)$$

where J_i is the flux of component i ; ΔC_i is the bulk concentration difference of component i ; K_i , overall mass transfer coefficient, can be related to the individual mass transfer resistance due to gas phase, membrane phase, and liquid phase [5].

$$\frac{1}{K_i} = \frac{H_i}{k_{g,i}} + \frac{H_i}{k_{m,i}} + \frac{1}{k_{l,i}} \quad (2.6)$$

where $k_{g,i}$, $k_{m,i}$, $k_{l,i}$ represent the mass transfer coefficient in gas, membrane and liquid phase respectively; H_i denotes the dimensionless Henry's constant ($C_{g,i}H_i = C_{l,i}$). Because $k_{g,i}$ and $k_{m,i}$ are much higher than $k_{l,i}$, the membrane and the gas phase resistance can be neglected in nonwetted gas absorption, that is, mass transfer is controlled by liquid phase under this mode.

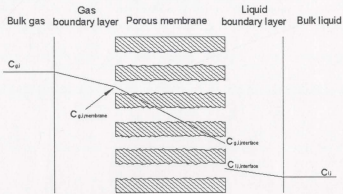


Figure 2. 7 Mass transfer regions in a membrane contactor

Chapter 3

Mathematical Models

In this chapter, mathematical models are developed to predict the mass transfer performance for both proposed dual-membrane contactors (Configuration 1 and 2) and an ordinary membrane contactor. A mixture of N_2 and CO_2 is used in the modeling with methanol as the absorbent liquid. Because N_2 does not take part in the absorption, the modeling reduces to a single-component absorption process. Actually, this simplified phenomenon never occurs in natural gas industry; hence multi-component absorption, which is the norm in sour gas treatment, will be discussed in Chapter 6.

3.1 Relevant Fluid Dynamics and Mass Transfer Fundamentals

3.1.1 Fully Developed Laminar Flow

Membrane contactors with flat-plate membranes are used in the modeling. Basic fluid dynamic fundamentals concerning flow between two parallel plates will be discussed as follows.

According to literatures, fully developed laminar flow in liquid phase is a reasonable assumption for the study of membrane contactors [3, 4 and 5], so we limit our study to the fully developed laminar flow in liquid phase in this thesis. Based on the coordinates in Figure 3-1, the following equations are derived [6]:

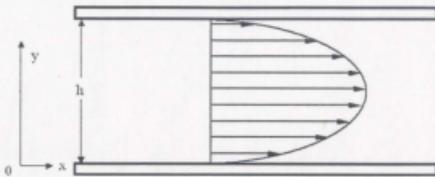


Figure 3. 1 Velocity profile for fully developed laminar flow between infinite parallel plates

The velocity can be expressed by:

$$u = \frac{h^2}{2\mu_l} \frac{dP_l}{dx} \left[\left(\frac{y}{h} \right)^2 - \left(\frac{y}{h} \right) \right] \quad (3.1)$$

where u denotes the velocity, μ_l denotes the viscosity of the liquid, and P_l denotes the pressure of the liquid. From the expression of velocity, we can see that velocity has a constant parabolic profile along the membrane, and is symmetrical in terms of centreline of the channel.

For the unit depth in z direction, the volume flow rate is given by:

$$Q = \int_0^h \frac{h^2}{2\mu_l} \frac{dP_l}{dx} \left[\left(\frac{y}{h} \right)^2 - \left(\frac{y}{h} \right) \right] dy = -\frac{1}{12\mu_l} \frac{dP_l}{dx} h^3 \quad (3.2)$$

The average velocity is given by:

$$\bar{u} = \frac{Q}{A} = -\frac{1}{12\mu_l} \frac{dP_l}{dx} \frac{h^3}{h} = -\frac{1}{12\mu_l} \frac{dP_l}{dx} h^2 \quad (3.3)$$

The maximum velocity is given by:

$$\text{At } y = \frac{h}{2}, u_{\max} = -\frac{1}{8\mu_l} \frac{dP_l}{dx} h^2 \quad (3.4)$$

Typically the gas is assumed in plug flow mode, which is an accurate simulation of real gas flow in membrane contactors [7].

3.1.2 Diffusion Mass Transfer

Mass is transported by the movement of a species in the direction of decreasing concentration, analogous to the heat conduction in the direction of decreasing temperature. Ordinary diffusion may occur in gases, liquids, and solids. Because of the different molecular spacing, the diffusion rate is faster in liquids than in solids, and is much more rapid in gases. The fundamental equation (one-dimensional) of diffusion for binary mixture can be written as follows:

$$J_A = -\rho D_{AB} \frac{\partial C_A}{\partial x} \quad (3.5)$$

where J_A is mass flux of species A relative to mass average velocity of mixture; ρ denotes mass density of the mixture; D_{AB} denotes the diffusion coefficient of species A with respect to species B ; C_A stands for mole concentration of species A . The proportionality factor, D_{AB} , or diffusion coefficient or diffusivity, is a physical property of specific system. Its value depends on the composition, temperature and pressure of system studied [8].

3.1.3 Convective Mass Transfer

In addition to transport by molecular motion, mass may also be transported by the bulk motion of the liquid, or convective mass transfer. The convective process can be either forced or natural, depending on the existence of a gradient of pressure or density in fluid.

In this thesis, only forced convective mass transfer in x direction and diffusive mass transfer in y direction are taken into account.

3.1.4 Governing Mass Transfer Equation

The general governing mass transfer equation for an incompressible flow can be written as:

$$\frac{\partial C_A}{\partial t} + u \frac{\partial C_A}{\partial x} + v \frac{\partial C_A}{\partial y} + w \frac{\partial C_A}{\partial z} = D_{AB} \left(\frac{\partial^2 C_A}{\partial x^2} + \frac{\partial^2 C_A}{\partial y^2} + \frac{\partial^2 C_A}{\partial z^2} \right) + R_A \quad (3.6)$$

For membrane contactors studied in this thesis, based on the assumptions which will be given later, the mass transfer model in liquid phase can be simplified as:

$$u \frac{\partial C_A}{\partial x} = D_{AB} \frac{\partial^2 C_A}{\partial y^2} \quad (3.7)$$

Combined with corresponding initial and boundary conditions, this model can be solved [8].

In gas phase, the concentration distribution of A in the y direction can be negligible compared to liquid phase since the diffusion coefficient in gas phase is typically much larger than in liquid phase. That is, gas phase is completely mixed in y direction and the concentration profile of component A in gas phase is a function of only x .

In the problems related to convective mass transfer, there are three combinations of velocity- and concentration-profile development [9]:

1. Developing velocity and concentration distributions. This condition prevails near the inlet to a tube or duct when mass transfer begins at the entrance.

2. Fully developed velocity distribution and developing concentration distribution. This set of conditions arises when the mass transfer starts far enough from the entrance to the pipe or duct that the velocity profile is fully developed.
3. Fully developed velocity and concentration distributions. These conditions are found at locations far downstream from the entrance to the tube and the mass transfer section.

In this thesis, the assumption that the velocity profile is fully developed makes our model under the condition 2, where the governing mass transfer equation is valid for both mass transfer entrance zone and fully developed zone. Thereby regardless of how long the mass transfer entrance length is, the model and solution is always valid.

3.2 Model Development:

The models are constructed based on the following assumptions:

1. The membranes are considered as infinite parallel plates
2. The membrane contactor is operated under steady state and isothermal conditions at 298.15 K.
3. The physical properties including diffusion coefficient, Henry's constant, density, viscosity etc. are constant along the membrane.
4. At the interface of gas and liquid, Henry' law is applicable, and equilibrium is instantaneously obtained.
5. The pressure in gas phase is constant along the membrane.
6. The liquid flow between two plates is fully developed laminar flow.
7. The x -direction diffusion and y -direction convection are negligible.

8. The membranes are under the nonwetted mode (gas-filled pores).

In addition, in Configuration 1 pure N_2 is used as sweeping gas. In Configuration 2, the solvent will inevitably evaporate through desorption membrane due to the low pressure employed on permeate side, so a nonporous membrane with a low permeability to the solvent should be chosen to make the vaporization negligible compared to the flux of CO_2 . Both counter current and co-current conditions are studied. CO_2 is denoted by A in the following formula.

3.2.1 Configuration 1

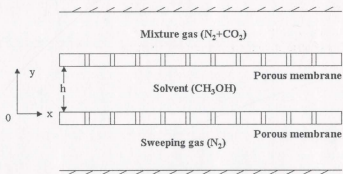


Figure 3. 2 Schematic arrangement of membranes in Configuration 1

Taking a differential segment of the mixture gas side of the upper porous membrane, according to material balance, the moles of CO_2 absorbed by solvent is equal to that diffusing through the boundary.

$$-dN_{g1} = w dx D_{At} \left. \frac{\partial C_{At}}{\partial y} \right|_{y=h} \quad (3.8)$$

where $w dx$ is the contact area, and N_{g1} denotes the molar flow rate of mixture gas.

Writing N_{g1} in terms of molar concentration:

$$N_{g1} = Q_{g1} C_{Ag1} \quad (3.9)$$

and neglecting the changing of Q_{g1} along the membrane, we can write

$$dN_{g1} = Q_{g1} dC_{Ag1} \quad (3.10)$$

Thereby, we have the equation:

$$-Q_{g1} \frac{dC_{Ag1}}{dx} = w D_{Al} \left. \frac{\partial C_{Al}}{\partial y} \right|_{y=h} \quad (3.11)$$

Based on the assumption that Henry's law is applicable at the boundary,

$$H_A C_{Ag1} = C_{Al} \quad (3.12)$$

we have the following equation:

$$-\frac{Q_{g1}}{H_A} \left. \frac{\partial C_{Al}}{\partial x} \right|_{y=h} = w D_{Al} \left. \frac{\partial C_{Al}}{\partial y} \right|_{y=h} \quad (3.13)$$

This expression can be taken as the boundary condition on the mixture gas side. Similarly, we can get the boundary condition on the sweeping gas side:

$$\frac{Q_{g2}}{H_A} \left. \frac{\partial C_{Al}}{\partial x} \right|_{y=0} = w D_{Al} \left. \frac{\partial C_{Al}}{\partial y} \right|_{y=0} \quad (3.14)$$

When combined with the governing partial differential equation in liquid phase, we have the following partial differential equation and initial and boundary conditions:

$$u \frac{\partial C_{Al}}{\partial x} = D_{Al} \frac{\partial^2 C_{Al}}{\partial y^2} \quad (3.15)$$

where

$$u = \frac{h^2}{2\mu_l} \frac{dP_l}{dx} \left[\left(\frac{y}{h} \right)^2 - \left(\frac{y}{h} \right) \right] \quad (3.16)$$

Inlet condition:

$$x = 0, \quad C_{A_l} = C_{A_l, \text{in}} \quad (3.17)$$

Boundary conditions:

$$y = 0, \quad \frac{Q_{g2}}{H_A} \frac{\partial C_{A_l}}{\partial x} \Big|_{y=0} = wD_{A_l} \frac{\partial C_{A_l}}{\partial y} \Big|_{y=0} \quad (3.18)$$

$$y = h, \quad -\frac{Q_{g1}}{H_A} \frac{\partial C_{A_l}}{\partial x} \Big|_{y=h} = wD_{A_l} \frac{\partial C_{A_l}}{\partial y} \Big|_{y=h} \quad (3.19)$$

3.2.2 Configuration 2

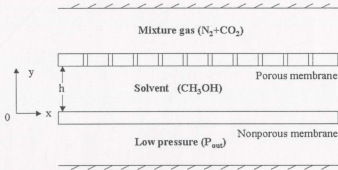


Figure 3. 3 Schematic arrangement of membranes in Configuration 2

The boundary condition on the mixture gas side can be obtained in the same way as in Configuration 1. For the nonporous membrane, we keep a constant CO_2 pressure (P_{out}) on the permeate side of the membrane. The molar flow rate of CO_2 diffusing out through nonporous membrane is denoted by N_{g2} .

$$\frac{dN_{g2}}{wdx} = D_{Al} \frac{\partial C_{Al}}{\partial y} \Big|_{y=0} \quad (3.20)$$

Meanwhile

$$\frac{dN_{g2}}{wdx} = Per_A (P^* - P_{out}) / \delta \quad (3.21)$$

where δ denotes the thickness of nonporous membrane; Per_A denotes the permeability of nonporous membrane with respect to CO_2 ; P^* denotes CO_2 partial pressure in equilibrium with the CO_2 concentration in solvent at the interface. Combing equation 3.20 and 3.21, we have

$$D_{Al} \frac{\partial C_{Al}}{\partial y} \Big|_{y=0} = Per_A (P^* - P_{out}) / \delta \quad (3.22)$$

According to Henry's law:

$$C_{Al}(x,0) = H_A C_{Ag}^* \quad (3.23)$$

$$C_{Ag}^* = \frac{P^*}{RT} \quad (3.24)$$

$$C_{Al}(x,0) = H_A \frac{P^*}{RT} \quad (3.25)$$

$$P^* = \frac{C_{Al}(x,0)RT}{H_A} \quad (3.26)$$

The resulting boundary condition on the nonporous membrane side is

$$D_{Al} \frac{\partial C_{Al}}{\partial y} \Big|_{y=0} = Per_A \left(\frac{C_{Al}(x,0)RT}{H_A} - P_{out} \right) / \delta \quad (3.27)$$

The governing equation in solvent phase and upper boundary condition derived in Configuration 1 are still valid here, so we have the following equations:

$$u \frac{\partial C_{A1}}{\partial x} = D_{A1} \frac{\partial^2 C_{A1}}{\partial y^2} \quad (3.28)$$

where

$$u = \frac{h^2}{2\mu_1} \frac{dP_1}{dx} \left[\left(\frac{y}{h} \right)^2 - \left(\frac{y}{h} \right) \right] \quad (3.29)$$

Inlet condition:

$$x = 0, \quad C_{A1} = C_{A1,in} \quad (3.30)$$

Boundary conditions:

$$y = 0, \quad D_{A1} \frac{\partial C_{A1}}{\partial y} \Big|_{y=0} = Per_A \left(\frac{C_{A1}(x,0)RT}{H_A} - P_{out} \right) / \delta \quad (3.31)$$

$$y = h, \quad -\frac{Q_g}{H_A} \frac{\partial C_{A1}}{\partial x} \Big|_{y=h} = wD_{A1} \frac{\partial C_{A1}}{\partial y} \Big|_{y=h} \quad (3.32)$$

3.2.3 Ordinary Membrane Contactor

To compare the novel dual-membrane contactors with ordinary single-membrane contactor, the ordinary membrane contactor is also modeled.

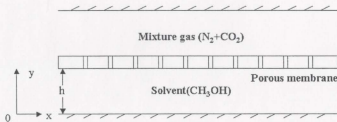


Figure 3. 4 Schematic drawing of ordinary membrane contactor

The governing equation in the liquid phase and boundary condition on the mixture gas side in Configuration 1 can be carried over here. The lower boundary condition is quite straightforward because there is no mass transfer across this boundary.

$$y = 0, \quad D_{Al} \frac{\partial C_{Al}}{\partial y} \Big|_{y=0} = 0 \quad (3.33)$$

Thereby we have the following equations:

$$u \frac{\partial C_{Al}}{\partial x} = D_{Al} \frac{\partial^2 C_{Al}}{\partial y^2} \quad (3.34)$$

where

$$u = \frac{h^2}{2\mu_l} \frac{dP_l}{dx} \left[\left(\frac{y}{h} \right)^2 - \left(\frac{y}{h} \right) \right] \quad (3.35)$$

Inlet condition:

$$x = 0, \quad C_{Al} = C_{Al,0} \quad (3.36)$$

Boundary conditions:

$$y = 0, \quad \frac{\partial C_{Al}}{\partial y} \Big|_0 = 0 \quad (3.37)$$

$$y = h, \quad -\frac{Q_g}{H_A} \frac{\partial C_{Al}}{\partial x} \Big|_{y=h} = wD_{Al} \frac{\partial C_{Al}}{\partial y} \Big|_{y=h} \quad (3.38)$$

For all the above three configurations, the mixture gas can flow in a co-current or a counter current scheme with the solvent. Under co-current condition, $Q_{g1}(Q_g)$ is positive

and $C_{Ag1}(C_{Ag})$ (inlet concentration of mixture gas) is given at $x=0$. Under counter current condition, $Q_{g1}(Q_g)$ is negative and $C_{Ag1}(C_{Ag})$ is given at $x=L$.

Chapter 4

Solutions to Model Equations

The objective of this chapter is to solve the partial differential equation developed in previous chapter, and demonstrate the proposed dual-membrane configurations can improve the performance of the ordinary single-membrane contactor. Firstly, the partial differential equation is solved numerically with Crank-Nicholson technique. The CO_2 removal efficiency of the novel dual-membrane contactors and that of the ordinary single-membrane contactor are compared and analysis shows that the novel proposed configurations remove CO_2 from $\text{CO}_2\text{-N}_2$ mixture gas more efficiently compared to the ordinary membrane contactor. Based on the consideration of a typical industrial application, Configuration 2 has more potential for practical application in gas industry. Then Configuration 2 is modeled with “bulk concentration” approach to check the accuracy of the partial differential equation and numerical solutions. This further demonstrates the novel dual-membrane contactor can improve the performance of the ordinary membrane contactor. Finally, in an attempt to verify the numerical solution analytically, the boundary conditions of the model are simplified to make the analytical solution available. The analytical solution to the model with simplified boundary conditions proved the Matlab code concerning partial differential equation part was correct.

4.1 Numerical Solution

It is known that not all partial differential equations can be solved analytically and that numerical solution can be a very good approximation if implemented correctly. The complexity of the partial differential equation and boundary conditions makes the numerical method preferable for this problem. The method used here is finite difference method in which derivatives of a function are replaced by difference equations. Both explicit and implicit methods can be used in the solving of the partial differential equations. Implicit method provides more accuracy, so the Crank-Nicholson method is used in the thesis. From the solution, the concentration distribution of the CO₂ in every phase can be obtained.

The Crank-Nicholson has the following advantages [10]:

1. It is unconditionally stable for linear partial differential equation.
2. It is second order in time variable
3. The influence of the boundary condition can be felt at all spatial points at a given time level.

4.1.1 Application of the Crank-Nicholson Method

The Crank-Nicholson method is explained in Appendix B. Now we apply the Crank-Nicholson method to solve the three models presented previously. The only difference among the three mathematical models (Configuration 1, Configuration 2, and single membrane contactor) is that they have different lower boundary conditions.

The first step is to discretize the domain by placing a grid over the domain. As shown in Figure 4.1, the grid spacing Δx is denoted as k , and Δy is denoted as h . Now the domain of the problem is approximated by the lattice of points. The solution to the problem can be approximated at the points on the lattice.

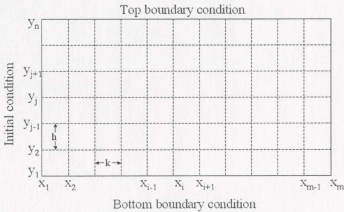


Figure 4. 1 Grid on solvent domain

Based on the partial differential equation:

$$u(y) \frac{\partial C_{Al}}{\partial x} = D_{Al} \frac{\partial^2 C_{Al}}{\partial y^2} \quad (4.1)$$

where

$$u(y) = \frac{h^2}{2\mu_1} \frac{dP_l}{dx} \left[\left(\frac{y}{h} \right)^2 - \left(\frac{y}{h} \right) \right] \quad (4.2)$$

we can write the difference scheme:

$$u((j-1)h) \frac{C_{i+1,j} - C_{i,j}}{k} = D_l \frac{C_{i+1,j-1} - 2C_{i+1,j} + C_{i+1,j+1} + C_{i,j-1} - 2C_{i,j} + C_{i,j+1}}{2h^2} \quad (4.3)$$

The rearranged form is

$$-\lambda C_{i+1,j-1} + (2\lambda + 2u((j-1)h))C_{i+1,j} - \lambda C_{i+1,j+1} = \lambda C_{i,j-1} + (2u((j-1)h) - 2\lambda)C_{i,j} + \lambda C_{i,j+1} \quad (4.4)$$

where

$$\lambda = c^2 k / h^2, \quad i = 1, 2, 3, \dots, m-1, \quad j = 2, 3, \dots, n-1 \quad (4.5)$$

For the upper boundary condition:

$$-\frac{Q_g}{H_A} \frac{\partial C_{Al}}{\partial x} \Big|_{y=h} = wD_{Al} \frac{\partial C_{Al}}{\partial y} \Big|_{y=h} \quad (4.6)$$

at the point $(i+1, n)$, based on backward difference method, the formulas:

$$\frac{\partial C_{Al}}{\partial x} \Big|_{y=h} = \frac{C_{i+1,n} - C_{i,n}}{k} + O(k) \quad (4.7)$$

and

$$\frac{\partial C_{Al}}{\partial y} \Big|_{y=h} = \frac{C_{i+1,n} - C_{i+1,n-1}}{h} \quad (4.8)$$

can be obtained, so the difference scheme can be written as:

$$-\frac{Q_g}{H_A} \frac{C_{i+1,n} - C_{i,n}}{k} = wD_{Al} \frac{C_{i+1,n} - C_{i+1,n-1}}{h} \quad (4.9)$$

The rearranged form is

$$C_{i+1,n-1} + \left(-\frac{Q_g h}{H_A k w D_{Al}} - 1\right) C_{i+1,n} = -\frac{Q_g h}{H_A k w D_{Al}} C_{i,n}, \quad i = 1, 2, 3, \dots, m-1 \quad (4.10)$$

For the lower boundary condition in Configuration 1:

$$y = 0, \quad \frac{Q_{g2}}{H_A} \frac{\partial C_{Al}}{\partial x} \Big|_{y=0} = wD_{Al} \frac{\partial C_{Al}}{\partial y} \Big|_{y=0} \quad (4.11)$$

the difference scheme for this boundary equation can be obtained in the same way for top boundary condition.

$$\frac{Q_{g2}}{H_A} \frac{C_{i+1,1} - C_{i,1}}{k} = wD_{Al} \frac{C_{i+1,2} - C_{i+1,1}}{h} \quad (4.12)$$

After rearranging, we have

$$\left(\frac{Q_{g2}h}{H_A k w D_{Al}} + 1 \right) C_{i+1,1} - C_{i+1,2} = \frac{Q_{g2}h}{H_A k w D_{Al}} C_{i,1} \quad (4.13)$$

For the lower condition in Configuration 2:

$$D_{Al} \left. \frac{\partial C_{Al}}{\partial y} \right|_{y=0} = P_{erA} \left(\frac{C_{Al}(x,0)RT}{H_A} - P_{out} \right) / \delta \quad (4.14)$$

at the point $(i+1,1)$, based on forward difference method, the formula:

$$\left. \frac{\partial C_{Al}}{\partial y} \right|_{y=0} = \frac{C_{i+1,2} - C_{i+1,1}}{h} \quad (4.15)$$

can be obtained, and $C_{Al}(x,0)$ can be denoted by $C_{i+1,1}$ so we have the following difference scheme:

$$D_{Al} \frac{C_{i+1,2} - C_{i+1,1}}{h} = P_{erA} \left(\frac{C_{i+1,1}RT}{H_A} - P_{out} \right) / \delta, \quad i = 1, 2, 3, \dots, m-1 \quad (4.16)$$

For the lower boundary condition in the ordinary membrane contactor:

$$y = 0, \quad D_{Al} \left. \frac{\partial C_{Al}}{\partial y} \right|_{y=0} = 0 \quad (4.17)$$

at the point $(i+1,1)$, based on forward difference method, the formula:

$$\left. \frac{\partial C_{Al}}{\partial y} \right|_{y=0} = \frac{C_{i+1,2} - C_{i+1,1}}{h} \quad (4.18)$$

can be obtained, so we have

$$C_{i+1,1} = C_{i+1,2} \quad (4.19)$$

Combining the difference schemes of partial differential equation and initial and boundary conditions, a Matlab program was designed to solve the models numerically. For the co-current flow, C_{Ag1} (or C_{Ag}) is given at the point (x_1, n) , so it is quite straightforward for Matlab to repeatedly implement the matrix calculation from x_2 through x_m . For the counter current flow, C_{Ag1} (or C_{Ag}) is given at the point (x_m, n) , so we need to assume an initial value at the point (x_1, n) . Then check the calculated value at the point (x_m, n) with given C_{Ag1} (or C_{Ag}). If they are not in agreement, the initial estimate is changed and the calculation repeated.

The assumed values of parameters used in the following calculations are listed in Table 4.1. It should be mentioned that the concentration distribution in the solvent in y direction is not of interest, so the formula:

$$\overline{C_{A1}} = \frac{\int_b^a u(y)C_{A1}(x, y)dy}{\int_b^a u(y)dy} \quad (4.20)$$

is used to get the average CO_2 concentration in the solvent phase. Thereby, CO_2 concentration in the solvent phase shown in the following diagrams will be a function of only x .

Table 4. 1 Parameters used in calculations

Parameter	Value
Channel height (m)	0.001
Dimension of membrane (m ²)	0.165×0.165
Solvent (methanol) flow rate (10 ⁻⁸ m ³ /s)	7.12
Mixture gas flow rate (10 ⁻⁷ m ³ /s)	6.25
CO ₂ inlet concentration (kgmol/m ³)	0.4034 (20% v)
Henry's constant (CO ₂ in methanol)	3.89 (Henry's law: $C_{ig} H_1 = C_{il}$)
Diffusivity of CO ₂ in methanol (10 ⁻⁹ m ² /s)	8.37
Pressure of mixture gas (10 ⁶ PaA)	5.0
Temperature (K)	298.15
Sweeping gas flow rate (10 ⁻⁷ m ³ /s)	1.5625 (Configuration 1)
Permeability of nonporous membrane (barrer)	33100
Pressure (permeate side) (10 ⁵ PaA)	2.0 (Configuration 2)

4.1.2 Configuration 1

Under co-current conditions, according to the numerical solution, the CO₂ concentration in the mixture gas decreases from 0.4034 to 0.2397 kgmol/m³, the average CO₂ concentration in the solvent increases from 0 to 0.9194 kgmol/m³, and the CO₂ concentration in the sweeping gas increases from 0 to 0.2380 kgmol/m³. Under counter current conditions, the CO₂ concentration in the mixture gas decreases from 0.4034 to

0.1572 kgmol/m³, the average CO₂ concentration in the solvent increases from 0 to 1.4123 kgmol/m³, and the CO₂ concentration in the sweeping gas increases from 0 to 0.3426 kgmol/m³ (See Table 4.2).

Table 4. 2 CO₂ inlet and outlet concentration for Configuration 1

CO ₂ Concentration	C _{in} (kgmol/m ³)	C _{out} (co-current) (kgmol/m ³)	C _{out} (counter current) (kgmol/m ³)
Mixture gas	0.4034	0.2397	0.1572
Solvent	0	0.9194	1.4123
Sweeping gas	0	0.2380	0.3426

It is clear from Table 4.2 that counter current flow pattern gives better CO₂ removal performance with the same solvent and sweeping gas flow rate. However, it should also be noticed that solvent from the counter current model is richer in CO₂ than that from co-current model. This may result in a higher duty on the solvent regeneration unit. Figure 4.2 and Figure 4.3 show the CO₂ concentration profiles under co-current and counter current conditions, respectively.

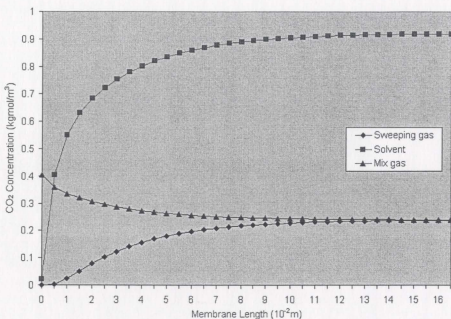


Figure 4. 2 CO₂ concentration profiles under co-current flow conditions for Configuration 1

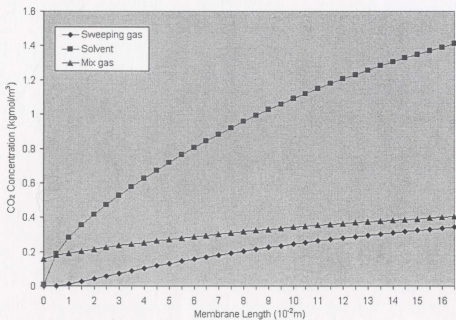


Figure 4. 3 CO₂ concentration profiles under counter current flow conditions for Configuration 1

4.1.3 Configuration 2

Under co-current conditions, the CO₂ concentration in the mixture gas decreases from 0.4034 to 0.1628 kgmol/m³, and the average CO₂ concentration in solvent increases from 0 to 0.4886 kgmol/m³. Under counter current conditions, the CO₂ concentration in the mixture gas decreases from 0.4034 to 0.1235 kgmol/m³, and the average CO₂ concentration in solvent increases from 0 to 0.9921 kgmol/m³ (See Table 4.3).

Table 4. 3 CO₂ inlet and outlet concentration for Configuration 2

CO ₂ Concentration	C _{in} (kgmol/m ³)	C _{out} (co-current) (kgmol/m ³)	C _{out} (counter current) (kgmol/m ³)
Mixture gas	0.4034	0.1628	0.1235
Solvent	0	0.4866	0.9291

Comparing these two models based on Table 4.3, the counter current flow pattern has a better CO₂ removal performance with the same flow rate of solvent and permeate side pressure. Figure 4.4 and Figure 4.5 show the CO₂ concentration profiles under co-current and counter current conditions, respectively.

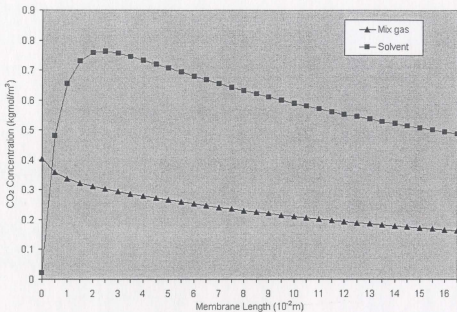


Figure 4. 4 CO₂ concentration profiles under co-current flow conditions for Configuration 2

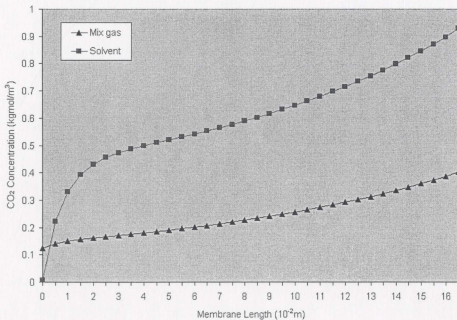


Figure 4. 5 CO₂ concentration profiles under counter current flow conditions for Configuration 2

4.1.4 Ordinary Membrane Contactor

For the co-current model, the CO_2 concentration in mixture gas decreases from 0.4034 to 0.2808 kgmol/m^3 , and the average CO_2 concentration in solvent increases from 0 to 1.0813 kgmol/m^3 . The counter current model indicates that the CO_2 concentration in the mixture gas decreases from 0.4034 to 0.2277 kgmol/m^3 , while the average CO_2 concentration in the solvent increases from 0 to 1.545 kgmol/m^3 (See Table 4.4). Again counter current flow pattern has the superior CO_2 removal performance. Figure 4.6 and Figure 4.7 show the CO_2 concentration profiles under co-current and counter current conditions, respectively.

Table 4. 4 CO_2 inlet and outlet concentration for ordinary membrane contactor

CO_2 Concentration	C_{in} (kgmol/m^3)	C_{out} (co-current) (kgmol/m^3)	C_{out} (counter current) (kgmol/m^3)
Mixture gas	0.4034	0.2808	0.2277
Solvent	0	1.0813	1.545

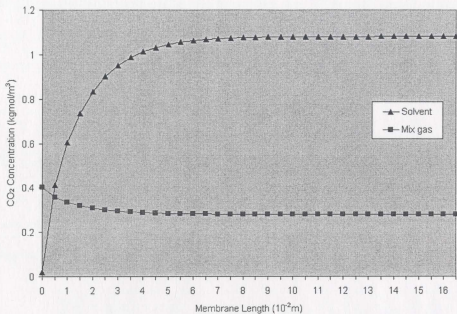


Figure 4. 6 CO₂ concentration profiles under co-current flow conditions for ordinary membrane contactor

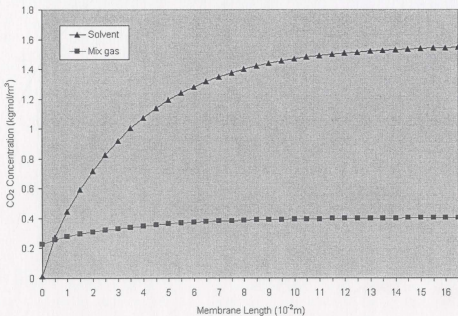


Figure 4. 7 CO₂ concentration profiles under counter current flow conditions for the ordinary membrane contactor

The comparison of CO₂ removal efficiencies between co-current and counter current flow patterns for the above membrane contactors has shown counter current flow can result in a better CO₂ removal performance, thereby, in the rest of this chapter, only counter current flow pattern is considered.

4.1.5 Comparison and Analysis

Figure 4.8 and Figure 4.9 show the CO₂ concentration profiles in mixture gas and solvent under counter current condition for Configuration 1, Configuration 2 and the ordinary membrane contactor.

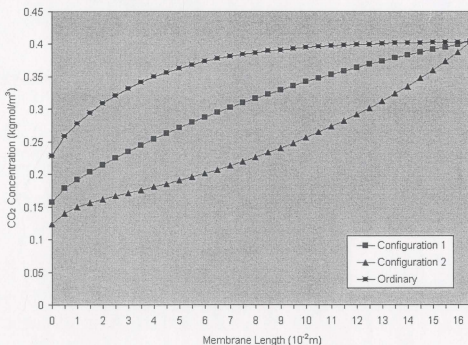


Figure 4. 8 CO₂ concentration profiles in mixture gas under counter current flow conditions

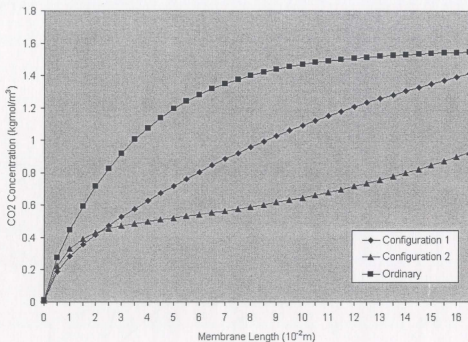


Figure 4.9 CO₂ concentration profiles in solvent under counter current flow conditions

Both Configuration 1 and Configuration 2 show advantages over the ordinary single-membrane contactor. The dual-membrane contactors can improve CO₂ removal performance by 1.7–2 times compared to the ordinary membrane contactor under the same solvent flow rate. In addition, the outlet CO₂ concentration in the solvent from either dual-membrane contactor is lower than that from the ordinary single-membrane contactor, which can potentially make regeneration of solvent less costly. The diagrams also show that Configuration 2 is preferable to Configuration 1 in terms of outlet CO₂ concentration in both mixture gas and solvent phase. Nevertheless, it cannot generally be concluded that Configuration 2 is a better choice, because if the sweeping gas flow rate is increased, a better CO₂ removal performance can also be achieved with Configuration 1.

However, Configuration 2 is a more practical choice than Configuration 1. The first reason is that applying a low pressure on the permeate side of the nonporous membrane, in many applications, is an easier task compared to finding the suitable source for the sweeping gas. In addition, the flow rate of permeate gas from Configuration 2 is much smaller than that of sweeping gas, which make it easier to dispose of. Thereby, we focus our study on Configuration 2 in the rest of the thesis.

4.2 Bulk Concentration Method

In addition to partial differential equation method, there is another method to model the novel membrane contactor. In this method, we neglect the concentration distribution in y direction in the liquid phase, and introduce a bulk concentration, or an average concentration, and mass transfer coefficient. Mass transfer flux can be expressed by:

$$J_i = k(C_{ib} - C_{i^*}) \quad (4.21)$$

where J_i is the flux of the component i , k is the boundary layer mass transfer coefficient for liquid phase, and C_{ib} and C_{i^*} denote the bulk concentration and interface concentration, respectively. k can be calculated analytically only in very simple situations; it is more commonly obtained through empirical correlations which can be found in the literature. Using the concept of overall mass transfer coefficient and the bulk concentration, a set of ordinary differential equations for each phase (mixture gas, solvent, and sweeping gas) in the membrane contactors can be established. These ordinary differential equations are coupled together, so they have to be solved simultaneously to get the concentration profiles. It should also be noted that the accuracy of the result could be affected due to the use of empirical correlation to estimate k .

For the mass transfer from gas to liquid (, and vice versa,) through a porous membrane, the mass transfer coefficient in liquid phase, or k_l , can be assumed to be also the overall mass transfer coefficient because the mass transfer is liquid-controlled. For mass transfer through a nonporous membrane from liquid to gas, a three-step mechanism is schematically shown in Figure 4.10

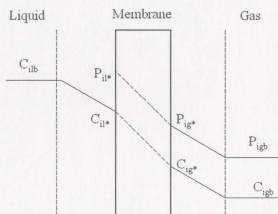


Figure 4. 10 Schematic drawing of component i transfer through nonporous membrane

The permeation flux on the liquid side can be written as:

$$J_i = k_l(C_{ilb} - C_{il*}) \quad (4.22)$$

The flux through the nonporous membrane can be described as:

$$J_i = \frac{Per_i}{\delta}(P_{il*} - P_{ig*}) \quad (4.23)$$

where Per_i is the permeability of the membrane with respect to component i , δ is the thickness of the membrane, P_{il*} and P_{ig*} denote the interfacial partial pressure of

component i on the liquid side and permeate side respectively. C_{i^*} can be related to P_{i^*} by the following formula as discussed previously:

$$P_{i^*} = \frac{C_{i^*}RT}{H_i} \quad (4.24)$$

Therefore,

$$J_i = \frac{Per_l}{\delta} (P_{i^*} - P_{ig^*}) = \frac{Per_l}{\delta} \left(\frac{C_{i^*}RT}{H} - P_{ig^*} \right) \quad (4.25)$$

Similar to the liquid phase, the permeate flux on gas side can be described by:

$$J_i = k_g (C_{ig^*} - C_{igb}) = \frac{k_g}{RT} (P_{ig^*} - P_{igb}) \quad (4.26)$$

According to Wenchang Ji et al [11], the flux can be described in terms of overall mass transfer coefficient, bulk concentrations in liquid and gas phase.

$$J_i = K \left(\frac{C_{ib}}{H_i} - C_{igb} \right) \quad (4.27)$$

where K is the overall mass transfer coefficient, and based on the additive rule of mass transfer resistances, K can be described by the following formula:

$$\frac{1}{K_i} = \frac{1}{H_i k_l} + \frac{\delta}{Per_l RT} + \frac{1}{k_g} \quad (4.28)$$

The third term on the right hand side of the formula can be ignored in that mass transfer resistance in gas phase can be negligible compared to that in the membrane and the liquid phase. Hence we have

$$\frac{1}{K_i} = \frac{1}{H_i k_l} + \frac{\delta}{Per_l RT} \quad (4.29)$$

4.2.1 Modeling in Bulk Concentration Method

Based on overall mass transfer coefficient and bulk concentration concepts, the membrane contactor in Configurations 1 and 2, and the ordinary membrane contactor can be modeled as follows. Here we only model the counter current flow pattern.

Configuration 1

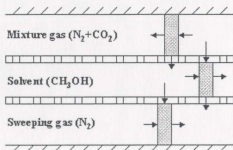


Figure 4.11 Bulk modeling schematic drawing for Configuration 1

Based on the control volume in the mixture gas phase, the following ordinary differential equation can be written:

$$-Q_{g1} \frac{dC_{Ag1}}{dx} = k_l w (H_A C_{Ag1} - C_{A1}) \quad (4.30)$$

$$x = L, C_{Ag1} = C_{Ag1,in} \quad (4.31)$$

Ordinary differential equation in the solvent phase can be written as:

$$Q_l \frac{dC_{A1}}{dx} = k_l w (H_A C_{Ag1} - C_{A1}) - k_l w (C_{A1} - H_A C_{Ag2}) \quad (4.32)$$

$$x = 0, C_{A1} = C_{A1,in} \quad (4.33)$$

Ordinary differential equation in the sweeping gas phase can be written as:

$$Q_{g2} \frac{dC_{Ag2}}{dx} = k_l W (C_{Al} - H_A C_{Ag2}) \quad (4.34)$$

$$x = 0, C_{Ag2} = C_{Ag2,in} \quad (4.35)$$

where L denotes the length of the membrane, Q denotes volume flow rate, and k_l can be obtained by this correlation [12]:

$$k_l = 0.816 \left(\frac{6Q_l D_l^2}{S^* h^2} \right)^{0.33} \quad (4.36)$$

where h denotes the height of the channel; S denotes the area of the membrane.

Equations 4.30–4.35 constitute a system of ordinary differential equations in terms of three unknown values C_{Ag1} , C_{Al} and C_{Ag2} . Maple* was used to solve the system of equations. All the parameters used are the same as those used in the numerical solution section and the value of k_l is calculated to be 9.446×10^{-6} m/s. Figure 4.12 shows the CO₂ concentration profiles in mixture gas, solvent, and sweeping gas phase.

* Maple is a comprehensive program for exploring, teaching, and applying mathematic, developed by Waterloo Maple Inc.

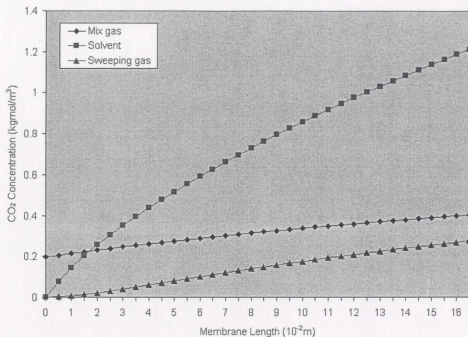


Figure 4. 12 CO₂ concentration profiles under counter current flow conditions for Configuration 1 based on “bulk concentration ” approach

Configuration 2

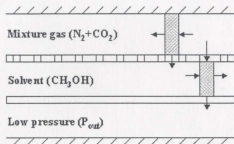


Figure 4. 13 Bulk modeling schematic drawing for Configuration 2

Similar to modeling for Configuration 1, the ordinary differential equation in the mixture gas phase can be written as:

$$-Q_g \frac{dC_{Ag}}{dx} = k_i w (H_A C_{Ag} - C_{Al}) \quad (4.37)$$

$$x = L, C_{Ag} = C_{Ag,in} \quad (4.38)$$

Ordinary differential equation in solvent phase can be written as:

$$Q_l \frac{dC_{Al}}{dx} = k_i w (H_A C_{Ag} - C_{Al}) - K_A w \left(\frac{C_{Al}}{H_A} - \frac{P_{out}}{RT} \right) \quad (4.39)$$

$$x = 0, C_{Al} = C_{Al,in} \quad (4.40)$$

Based on formula 4.29

$$K_A = 3.435 \times 10^{-5} \text{ m/s} \quad (4.41)$$

The two ordinary differential equations can be solved using Maple simultaneously, giving the following concentration profiles as follows.

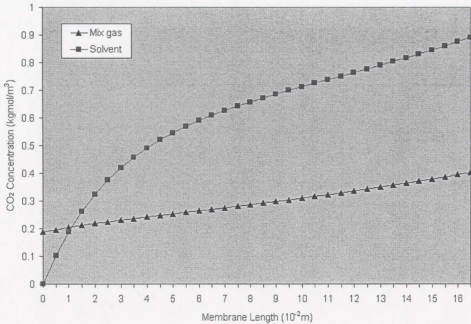


Figure 4. 14 CO₂ concentration profiles under counter current flow conditions for configuration 2 based on “bulk concentration” approach

Ordinary membrane contactor

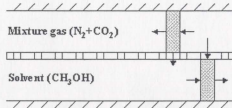


Figure 4. 15 Bulk modeling schematic drawing for ordinary membrane contactor

Ordinary differential equation in mixture gas phase can be written as:

$$-Q_g \frac{dC_{Ag}}{dx} = k_l w (H_A C_{Ag} - C_{Al}) \quad (4.42)$$

$$x = L, C_{Ag} = C_{Ag,in} \quad (4.43)$$

Ordinary differential equation in solvent phase can be written as:

$$Q_l \frac{dC_{Al}}{dx} = k_l w (H_A C_{Ag} - C_{Al}) \quad (4.44)$$

$$x = 0, C_{Al} = C_{Al,in} \quad (4.45)$$

The solutions by Maple are shown as follows.

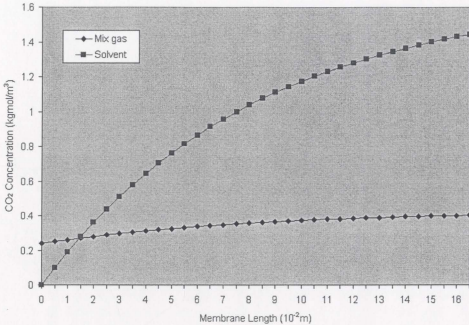


Figure 4. 16 CO₂ concentration profiles under counter current flow conditions for ordinary membrane contactor based on "bulk concentration " approach

4.2.2 Comparison of Three Configurations

Putting the CO₂ concentration profiles in mixture gas phase from Configuration 1, Configuration 2 and ordinary membrane contactors in the same diagram, we can see both Configuration 1 and Configuration 2 can give lower CO₂ outlet concentration compared with ordinary membrane contactor, that is, both methods can improve the performance of ordinary membrane contactor. This is the same conclusion as what we got from partial differential method previously (See Figure 4.17).

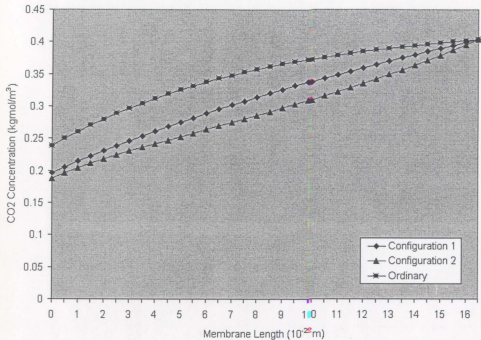


Figure 4. 17 CO₂ concentration profiles in mixture gas under counter current flow conditions based on “bulk concentration” approach

Comparing the CO₂ profiles from “bulk concentration” method with that from partial differential equation method respectively in Configurations 1 and 2 and the ordinary contactor, as shown in the Figure 4.18, 4.19 and 4.20, we can see both modeling methods show the same trend of CO₂ concentration changes although the profiles do not fall exactly on each other. The divergence between the two methods is believed to be due to the use of empirical equations to estimate the liquid phase mass transfer coefficient.

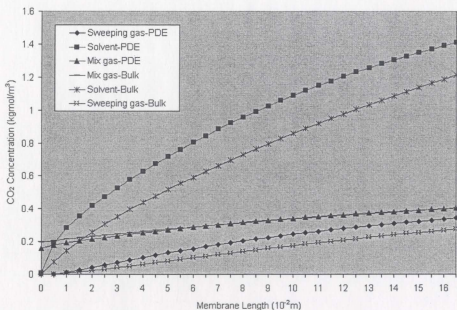


Figure 4.18 CO₂ concentration profiles under counter current flow conditions for Configuration 1

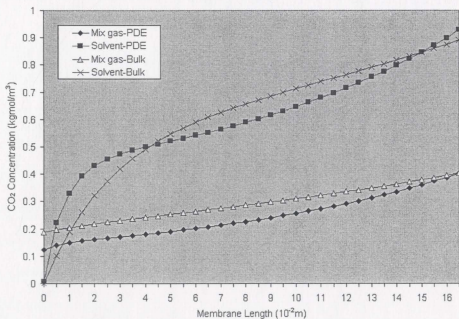


Figure 4.19 CO₂ concentration profiles under counter current flow conditions for Configuration 2

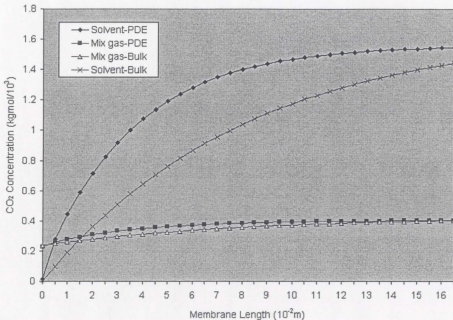


Figure 4.20 CO₂ concentration profiles under counter current flow conditions for ordinary membrane contactor

4.3 Analytical Solution

To further check the accuracy of the numerical solutions, we try to solve the partial differential equations analytically. Since the complicated boundary conditions make analytical solutions impossible, to solve the partial differential equations analytically, we simplify both boundary conditions to a constant mass transfer rate, M_0 , diffusing into the solvent phase. Now three configurations have the same simplified partial differential equation and initial and boundary conditions which can be solved asymptotically. Hence the numerical code associated with partial differential equation part can be checked in an analytical way.

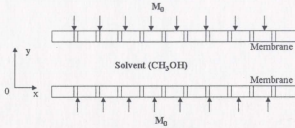


Figure 4. 21 Simplified membrane contactor

Simplified partial differential equation and initial and boundary conditions:

$$u \frac{\partial C_{Al}}{\partial x} = D_{Al} \frac{\partial^2 C_{Al}}{\partial y^2} \quad (4.45)$$

where

$$u = \frac{h^2}{2\mu_l} \frac{dP_l}{dx} \left[\left(\frac{y}{h} \right)^2 - \left(\frac{y}{h} \right) \right] \quad (4.46)$$

Based on formula 3.4, we have

$$-4u_{\max} \left[\left(\frac{y}{h} \right)^2 - \left(\frac{y}{h} \right) \right] \frac{\partial C_{Al}}{\partial x} = D_{Al} \frac{\partial^2 C_{Al}}{\partial y^2} \quad (4.47)$$

Inlet condition:

$$x = 0, \quad C_{Al} = C_{Al,in} \quad (4.48)$$

Boundary conditions:

$$y = 0, \quad D_{Al} \frac{\partial C_{Al}}{\partial y} \Big|_{y=0} = -M_0 \quad (4.49)$$

$$y = h, \quad D_{Al} \frac{\partial C_{Al}}{\partial y} \Big|_{y=h} = M_0 \quad (4.50)$$

4.3.1 Numerical Solution to Simplified Model

Table 4.5 gives the parameters used in the calculations. The Crank-Nicholson method is used in the numerical method. The average CO₂ concentration profile in solvent is shown in Figure 4.22.

Table 4.5 Parameters used in calculations

Paramter	Value
Channel height (m)	0.001
Dimension of membrane(m ²)	0.165×0.165
Solvent (Methanol) flow rate (10 ⁻⁸ m ³ /s)	7.12
Diffusivity of CO ₂ in Methanol (10 ⁻⁹ m ² /s)	8.37
M ₀ (10 ⁻⁷ kgmol/m ²)	5

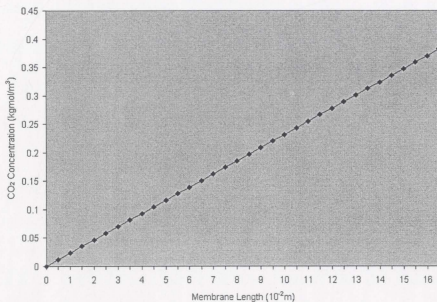


Figure 4. 22 CO₂ concentration in solvent profile from numerical solution

4.3.2 Analytical Solution (Asymptotic solution)

To minimize the number of parameters in manipulation, the formulas 4.47, 4.48, 4.49 and 4.50 are non-dimensionalized as follows:

$$(Y - Y^2) \frac{\partial C^*}{\partial X} = \frac{\partial^2 C^*}{\partial Y^2} \quad (4.51)$$

$$X = 0, \quad C^* = 0 \quad (4.52)$$

$$Y = 0, \quad \left. \frac{\partial C^*}{\partial Y} \right|_{Y=0} = -1 \quad (4.53)$$

$$Y = 1, \quad \left. \frac{\partial C^*}{\partial Y} \right|_{Y=1} = 1 \quad (4.54)$$

where

$$X = \frac{x}{4u_{\max} h^2 / D_{Al}} \quad (4.55)$$

$$C^* = \frac{C_{Al}}{hM_0 / D_{Al}} \quad (4.56)$$

$$Y = \frac{y}{h} \quad (4.57)$$

After the fluid flows far downstream from the beginning of mass transfer, that is

$$X \rightarrow \infty \quad (4.58)$$

two assumptions hold: one is that the constant mass transfer diffusing through membrane will result in a rise of concentration that is linear with X ; the other is that the shape of concentration profile as a function of Y will not undergo further change with the increasing X . Therefore, a solution of the following form seems quite reasonable for large X .

$$C^*(X, Y) = C_0 X + \psi(Y) \quad (4.59)$$

After substituting it into non-dimensionalized partial differential equation, we get

$$(Y - Y^2)C_0 = \frac{\partial^2 \psi}{\partial Y^2} \quad (4.60)$$

Integrating the above equation, we get

$$\psi(Y) = \frac{C_0}{6} Y^3 - \frac{C_0}{12} Y^4 + C_1 Y + C_2 \quad (4.61)$$

Thereby, the solution should be

$$C^*(X, Y) = C_0 X + \frac{C_0}{6} Y^3 - \frac{C_0}{12} Y^4 + C_1 Y + C_2 \quad (4.62)$$

where C_0, C_1, C_2 is constant.

The inlet condition cannot be applied to get the constant because of the precondition that X approaches infinity. Here we use an integral condition from conservation of mass.

$$2xM_0 = \int_0^1 uC dy \quad (4.63)$$

Dimensionless form:

$$2X = \int_0^1 C^*(Y - Y^2) dY \quad (4.64)$$

Applying boundary conditions and the extra condition leads to the asymptotic solution ($X \rightarrow \infty$):

$$C^*(X, Y) = 12X + 2Y^3 - Y^4 - Y + \frac{17}{70} \quad (4.65)$$

For small X ($X \rightarrow 0$), the mass transfer affects only a very thin region near the membrane, so the following two assumptions can be made to simplify the governing equation:

1. The fluid can be regarded as extending from the membrane ($y = 0$) to infinity ($y \rightarrow \infty$).
2. The velocity profile may be treated as linear, that is:

$$u = 2u_0 \frac{y}{h} \quad (4.66)$$

where

$$u_0 = 2u_{\max} \quad (4.67)$$

Then the governing partial differential equation can be simplified as:

$$4u_{\max} \frac{y}{h} \frac{\partial C_{Al}}{\partial x} = D_{Al} \frac{\partial^2 C_{Al}}{\partial y^2} \quad (4.68)$$

Initial and boundary conditions:

$$x = 0, \quad C_{Al} = 0 \quad (4.69)$$

$$y = 0, \quad D_{Al} \left. \frac{\partial C_{Al}}{\partial y} \right|_{y=0} = -M_0 \quad (4.70)$$

$$y \rightarrow \infty, \quad \frac{\partial C_{Al}}{\partial y} = 0 \quad (4.71)$$

From literature, we can get the analytical solution to above partial differential equation as [8]:

$$C^*(X, Y) = \sqrt[3]{36X} \left[\frac{\exp\left(-\frac{2Y^3}{9X}\right)}{\Gamma\left(\frac{2}{3}\right)} - \frac{2Y}{\sqrt[3]{36X}} \left(1 - \frac{\Gamma\left(\frac{2}{3}, \frac{2Y^3}{9X}\right)}{\Gamma\left(\frac{2}{3}\right)} \right) \right] \quad (4.72)$$

where X and Y have the same definition as previously, $\Gamma\left(\frac{2}{3}\right)$ is gamma function and

$\Gamma\left(\frac{2}{3}, \frac{2Y^3}{9X}\right)$ is incomplete gamma function.

The complete solution should be

$C^*(X, Y) =$

$$\left\langle \left\langle \sqrt[3]{36X} \left[\frac{\exp\left(-\frac{2Y^3}{9X}\right)}{\Gamma\left(\frac{2}{3}\right)} - \frac{2Y}{\sqrt[3]{36X}} \left(1 - \frac{\Gamma\left(\frac{2}{3}, \frac{2Y^3}{9X}\right)}{\Gamma\left(\frac{2}{3}\right)} \right) \right] \right\rangle \right\rangle^n + \left\langle 12X + 2Y^3 - Y^4 - Y + \frac{17}{70} \right\rangle^n \quad (4.73)$$

The value of n could be determined by experimental data to make the solution complete. However, for our particular problem, we pay little attention to the concentration very close to the beginning of mass transfer. Thereby we can just neglect the asymptotic solution ($x \rightarrow 0$) and approximate the analytical solution with the asymptotic solution ($x \rightarrow \infty$). Using the parameters given in Table 4.5, we calculate and get the CO_2 concentration profile shown in Figure 4.23.

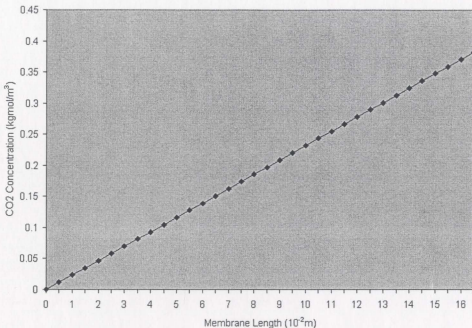


Figure 4. 23 CO₂ concentration in solvent profile from analytical solution

4.3.3 Comparison between Numerical and Analytical Solutions

Next we put the concentration profiles from two methods into the same figure. From Figure 4.24, we can see that both profiles fall together and the numerical solution is in a good agreement with asymptotic solution. That means the Matlab code concerning the partial differential equation part is right.

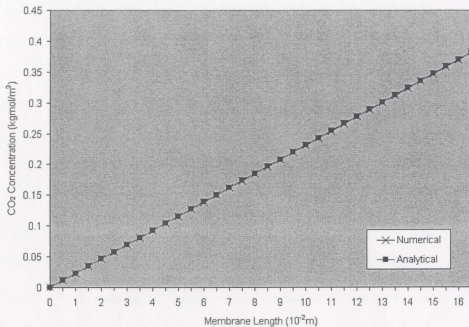


Figure 4. 24 CO₂ concentration in solvent profiles from analytical and numerical solutions

Chapter 5

Impact of Model Parameters on Performance

In this chapter, the effects of a variety of parameters, such as the channel height of solvent flow, the pressure applied on the permeate side, the Henry's constant, etc, on the efficiency of acid gas removal are examined. As demonstrated previously, both Configuration 1 and Configuration 2 can improve the CO₂ removal efficiency compared to the ordinary single-membrane contactor, but Configuration 2, the dual-membrane contactor with a nonporous second membrane, is more practical, so we limit our study on Configuration 2. By changing these parameters separately, we can get the information on the impacts of each parameter on the acid gas removal performance, which can subsequently lead to the optimal selection of parameters in the future follow-up experiments. In the following analyses the common parameters are kept the same as those used in previous chapters.

5.1 Channel Height

To examine the effect of solvent channel height on the acid gas removal performance, the channel height is adjusted by 0.0002 m beginning at 0.0006 m through 0.002 m. Both the novel dual-membrane contactor and the ordinary single-membrane contactor channel heights were adjusted and the outlet CO₂ concentrations in mixture gas were compared at different channel heights.

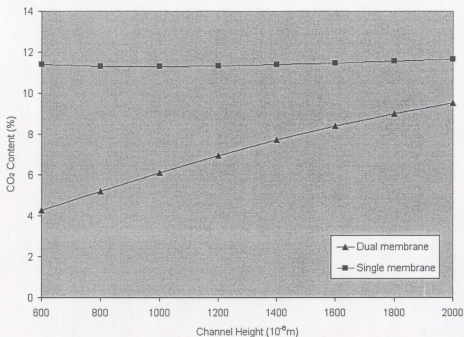


Figure 5. 1 The effect of channel height on acid gas removal

From Figure 5.1 the outlet CO₂ content curve for dual-membrane system is below that of single-membrane contactor, which means the novel dual-membrane system does improve the performance of the ordinary membrane contactor. In addition, it is obvious from the diagram that the channel height of solvent plays a significant role in the efficiency improvement. For the ordinary membrane contactor, the outlet CO₂ content in mixture gas remains around 11.5% regardless of the channel height. For the dual-membrane contactor, the outlet CO₂ content in mixture gas decreases significantly, changing from 9.5% to 4.3%, when the channel height of solvent decreases from 0.002 to 0.0006 m. This means the smaller the channel height, the greater the impact of the nonporous membrane, or an indication of a better removal performance for the novel dual-membrane contactor.

5.2 Permeate Side Pressure

To examine the effect of the permeate side pressure on the acid gas removal efficiency, the pressure is increased in 1.0×10^5 Pa increments starting from vacuum (0 PaA) through 7.0×10^5 PaA; the outlet CO_2 content in mixture gas for the novel contactor was compared with that for the ordinary membrane contactor at different permeate pressures.

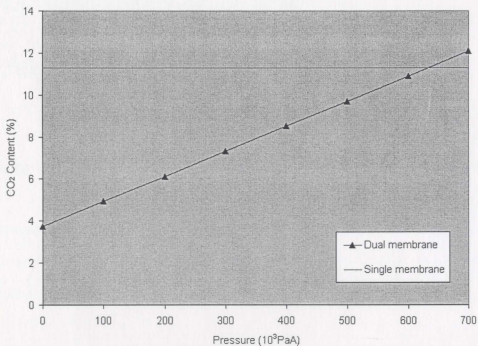


Figure 5.2 The effect of permeate side pressure on acid gas removal

From Figure 5.2 the CO_2 content in mixture gas leaving the dual-membrane increases from 3.7% to 12.1%, almost linearly with the increase of pressure. This indicates the lower the permeate side pressure, the better removal performance for the novel dual-membrane contactor. In addition, it should be noticed that the outlet CO_2 content of the

dual-membrane system can exceed that of the single-membrane system when the pressure increases (around 6.3×10^5 PaA in this case). This means the novel dual-membrane system can improve the performance of ordinary membrane contactors only when a positive differential pressure exists between the solvent side and the permeate side. Actually this is the requirement for all mass transfer devices. If this driving force requirement is not met, the mass transfer will reverse and the second membrane will impose a negative effect on the gas removal efficiency.

5.3 The Henry's Constant

It is known that the Henry's constant is a gas solubility parameter and depends on the type of solvent chosen for gas treating processes. It is also known that when the solvent is changed both the Henry's constant and diffusivity will change. However, to examine the effect that the Henry's constant poses on the acid gas removal performance, all the other parameters, including the diffusivity, are kept constant and the Henry's constant is increased from 2 through 11. By comparing the outlet CO_2 content of the two contactors at different Henry's constant values, the impact of Henry's constant can be assessed.

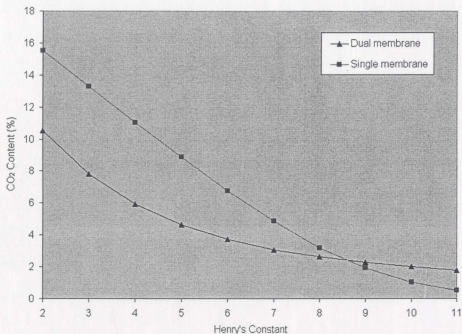


Figure 5.3 The effect of Henry's constant on acid gas removal

Both curves in Figure 5.3 show a decreasing trend when Henry's constant increase, which means both contactors show a better performance as the Henry's constant increases. In addition, these two curves intersect at a certain Henry's constant value (around 8.6 in this particular case). For Henry's constant before intersection, the dual-membrane contactor shows a better performance than the ordinary single membrane contactor; while for Henry's constant after intersection, the dual-membrane system results in a negative effect on the gas removal efficiency of the ordinary membrane contactor. The reason is that, at the solvent entrance, the CO₂ partial pressure on the permeate side is larger compared to the mixture gas side and causes a reverse concentration driving force, resulting in a reverse mass transfer from permeate side to the mixture gas side. Thereby, the novel dual-membrane idea can improve the efficiency of

the ordinary membrane contactor only in a certain range of Henry's constant value. Particular attention should be given to this issue in selection of the solvent and any subsequent engineering design work.

5.4 Diffusivity

Like in the previous section, the diffusivity is arbitrarily varied from 3×10^{-9} to 10×10^{-9} m^2/s with all the other parameters are kept constant to examine the effect that diffusivity individually poses on the acid gas removal performance. By comparing the outlet CO_2 content of the two contactors at different diffusivities, the impact of diffusivity on the contactor performance can be assessed.

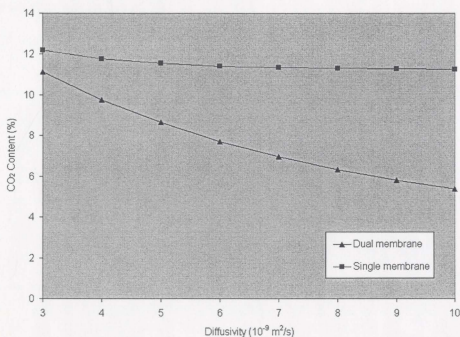


Figure 5. 4 The effect of diffusivity on acid gas removal

The dual-membrane curve is below the single-membrane curve, which means the dual-membrane contactor shows a better performance than the single-membrane contactor

regardless of the diffusivity. In addition, both curves show a decreasing trend when diffusivity increases, which means the removal efficiency of both contactors increases with the increase in diffusivity. In addition, the gap between the two curves gets larger when the diffusivity becomes larger. This means the greater the diffusivity, the more efficiency improvement can be expected from the dual-membrane contactor.

5.5 Solvent Flow Rate

To examine the effect of solvent flow rate on the acid gas removal performance, the flow rate is varied from 5.0×10^{-8} to 1.3×10^{-7} m³/s. By comparing the outlet CO₂ content of the two contactors at different solvent flow rates, the impact of solvent flow rate on the contactor can be assessed.

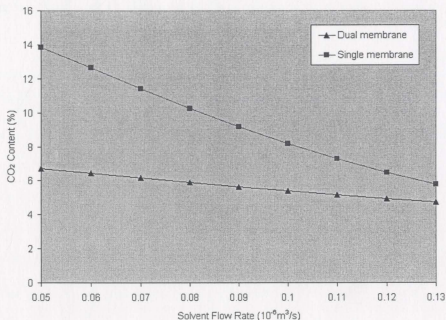


Figure 5. 5 The effect of solvent flow rate on acid gas removal

Firstly, the dual membrane curve is below single membrane curve, which means dual-membrane contactor does show a better performance compared to the ordinary membrane contactor. Secondly, both curves show a decreasing trend when flow rate increases, which means the removal efficiency of both contactors increases with the increase in solvent flow rate. In addition, dual membrane curve is less sensitive to the solvent flow rate and the gap between two curves gets smaller when the flow rate increases. That means the smaller the solvent flow rate, the better the removal efficiency improvement from the dual-membrane contactor can be expected. The reason is the diffusion through the second membrane becomes less controlling and less residence time is provided for partial regeneration of the solvent at higher flow rates and therefore better relative improvement can be seen when the flow rate is small. This is a very important factor when enhanced solvents formulated for acid gas removal purposes are considered in combination with a compact membrane contactor for gas processing facilities.

5.6 Permeability

To examine the effect of permeability on the acid gas removal performance, the permeability is varied from 500 to 50,000 Barrer with all other parameters constant. Because the variation in permeability is so large, 500 Barrer increment between 500 and 5,000 Barrer, and 5,000 Barrer increment between 5,000 and 50,000 Barrer are justified. The effect of permeability on the acid gas removal performance can be assessed by comparing the outlet CO_2 contents in mixture gas of both contactors.

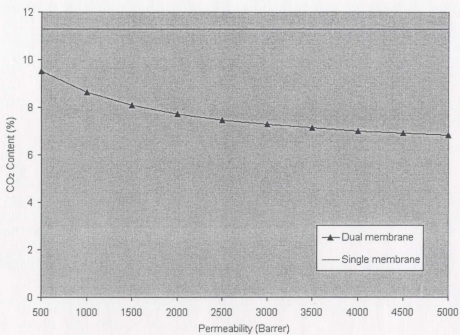


Figure 5.6 The effect of permeability on acid gas removal

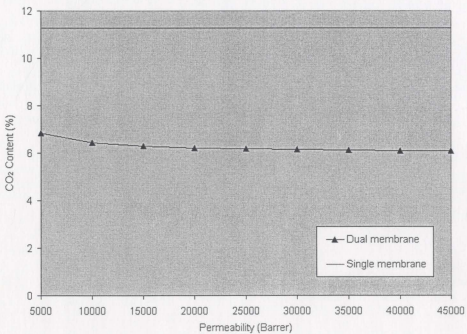


Figure 5.7 The effect of permeability on acid gas removal

When the permeability increases from 500 to 50,000 Barrer, the outlet CO₂ content in mixture gas of the dual-membrane contactor decreases from 9.5% through 6%, always below the value of single-membrane contactor. This means the larger the permeability, the better removal performance of the novel dual-membrane contactor. In addition, when the permeability changes from 500 to 5,000 Barrer, the CO₂ content decreases from 9.5% to 6.8%; however, when the permeability changes from 5,000 to 50,000 Barrer, the decrease is less dramatic, from 6.8% to 6.08%. This indicates that when permeability is larger than 5,000 Barrer, increasing permeability will not result in a significant improvement to the performance, so nonporous membrane with very high permeability (much higher than 5,000 Barrer) is not necessary when choosing the nonporous membrane in the engineering design.

5.7 Mixture Gas Pressure

To check the effect of mixture gas pressure on the performance, the mixture gas pressure was adjusted in 1.0×10^6 Pa increments ranging from 3.0×10^6 through 1.0×10^7 Pa. It should be noted that the inlet CO₂ content, rather than CO₂ molar concentration, was kept constant at 20% (vol). In addition, the actual volumetric flow rate of mixture gas, rather than the volumetric flow rate at standard conditions, was kept constant at 6.25×10^{-7} m³/s. Actually, the actual inlet CO₂ molar concentration and the molar amount of CO₂ entering the contactor are different at different pressures.

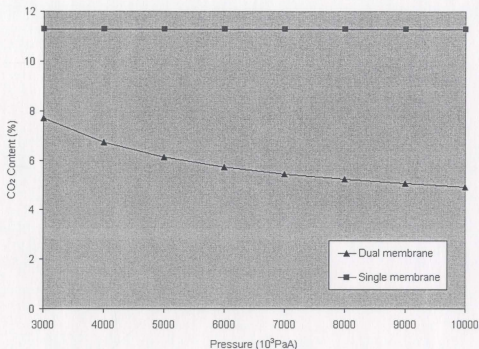


Figure 5. 8 The effect of mixture gas pressure on acid gas removal

When pressure increase from 3.0×10^6 to 1.0×10^7 PaA, the outlet CO₂ content in mixture gas of the dual-membrane system decreases from 7.7% to 4.9%; meanwhile, the outlet CO₂ content of single-membrane system remains constant at 11.3%. This means the performance of dual membrane contactor gets better with increase in operating pressure and dual-membrane contactor does show a better performance compared to ordinary membrane contactor. In addition, the gap between the two curves gets larger when the pressure increases, which means the larger the operating pressure, the better removal efficiency improvement from the dual-membrane contactor over the single-membrane contactor. It should be noted that the actual CO₂ molar amount absorbed into solvent increases when operating pressure increases. However, because the volumetric content,

instead of molar concentration, is used in the diagram, the outlet CO₂ content of the single-membrane contactor remains constant at different pressures.

In the above discussion only the individual parameter effects on the performance of the novel dual-membrane system have been studied. In real experiments or engineering design, certain parameters are dependent on one another and likely will interact with each other, which can lead to a rather more complicated situation. As such, a more extensive analysis is needed to obtain the optimum performance and economic value. In addition, all the above analysis is based on the CO₂ and methanol system, so when the solute or solvent changes, the optimum operating parameters will also change accordingly.

Chapter 6

Multi-component System

As demonstrated previously, the novel dual-membrane contactor can significantly improve the CO₂ removal efficiency from the mixture gas. However, natural gas is made up of many components. Thereby, to simulate acid gas removal of natural gas, the mathematical models discussed previously need some modifications to deal with the multi-component nature of natural gas. The mathematical model for multi-component system is developed and solved in this chapter to demonstrate how this novel dual-membrane contactor works for multi-component streams. As previous chapters have demonstrated, the counter current flow pattern has superior performance over co-current flow pattern, and therefore the focus will only be on Configuration 2 with counter current flow pattern.

6.1 Mathematical Model

In the model a multi-component system is considered in which n components participate in absorption. To simplify the analysis, component i is used to denote components $1, 2, 3, \dots, n$ (i.e. $i = 1, 2, 3, \dots, n$).

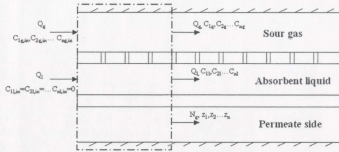


Figure 6. 1 Schematic drawing of multi-component absorption

Based on the single-component absorption model, for component i , we have the following partial differential equation and corresponding initial and boundary conditions:

$$\frac{h^2}{2\mu_i} \frac{dP_i}{dx} \left[\left(\frac{y}{h} \right)^2 - \left(\frac{y}{h} \right) \right] \frac{\partial C_{il}}{\partial x} = D_{il} \frac{\partial^2 C_{il}}{\partial y^2} \quad (6.1)$$

Inlet condition:

$$x = 0, C_{il} = 0 \quad (6.2)$$

Boundary conditions:

$$y = 0, D_{il} \frac{\partial C_{il}}{\partial y} \Big|_{y=0} = Per_i \left(\frac{C_{il}(x,0)RT}{H_i} - P_{out} z_i \right) / \delta \quad (6.3)$$

$$y = h, -\frac{Q_g}{H_i} \frac{dC_{il}}{dx} \Big|_{y=h} = wD_{il} \frac{\partial C_{il}}{\partial y} \Big|_{y=h} \quad (6.4)$$

where z_i denotes the mole fraction of component i in the permeate side. When n components participate in the absorption, we have n of the above partial differential equations. A mass balance over the control volume in Figure 6.1 for component i results in:

for component 1, mass balance:

$$Q_g C_{1g} + Q_l \bar{C}_{1l} + N_g z_1 = Q_g C_{1g,in} \quad (6.5)$$

for component 2, mass balance:

$$Q_g C_{2g} + Q_l \bar{C}_{2l} + N_g z_2 = Q_g C_{2g,in} \quad (6.6)$$

for component n , mass balance:

$$Q_g C_{ng} + Q_l \bar{C}_{nl} + N_g z_n = Q_g C_{ng,in} \quad (6.7)$$

The above n equations, together with the equation:

$$z_1 + z_2 + \dots + z_n = 1 \quad (6.8)$$

constitute a system of equations comprising $n+1$ equations with $n+1$ unknown values ($z_1, z_2, \dots, z_n, N_g$). Substituting z_1, z_2, \dots, z_n expressions into the preceding n partial differential equations, and applying Henry's law to convert C_{ig} into $C_{il}(x, h)$, results in a system of partial differential equations comprising n partial differential equations with the n unknown values ($C_{1l}, C_{2l}, \dots, C_{nl}$). This system can be solved numerically by the Crank-Nicholson technique similar to the previous chapter with Matlab and the concentration profile of component i in the solvent phase can be obtained; hence the concentration profile of any component in the mixture gas can also be obtained accordingly.

Acid components such as CO_2 and H_2S are the most common impurities found in raw natural gas. The acid components need to be removed before entering into the delivery pipeline to prevent corrosion. Methanol is chosen here to act as the absorbent liquid. The solubility of methane, which is the major component of natural gas, in methanol is

negligible compared to that of CO₂ and H₂S. As such this sweetening of natural gas is actually a two-component absorption process. The two-component absorption process can be modeled and the numerical solutions can be obtained as follows:

For CO₂, denoted as component 1:

$$Q_g C_{1g} + Q_l \bar{C}_{1l} + N_g z_1 = Q_g C_{1g,in} \quad (6.9)$$

For H₂S, denoted as component 2:

$$Q_g C_{2g} + Q_l \bar{C}_{2l} + N_g z_2 = Q_g C_{2g,in} \quad (6.10)$$

Meanwhile,

$$z_1 + z_2 = 1 \quad (6.11)$$

We have the following partial differential equation system.

For component 1:

$$\frac{h^2}{2\mu_l} \frac{dP_l}{dx} \left[\left(\frac{y}{h} \right)^2 - \left(\frac{y}{h} \right) \right] \frac{\partial C_{1l}}{\partial x} = D_{1l} \frac{\partial^2 C_{1l}}{\partial y^2} \quad (6.12)$$

Inlet condition:

$$x = 0, C_{1l} = 0 \quad (6.13)$$

Boundary conditions:

$$y = 0, D_{1l} \frac{\partial C_{1l}}{\partial y} \Big|_{y=0} = \frac{Per_1}{\delta} \left(\frac{C_{1l}(x,0)RT}{H_1} - P_{out} z_1 \right) \quad (6.14)$$

$$y = h, -\frac{Q_g}{H_1} \frac{dC_{1l}}{dx} \Big|_{y=h} = wD_{1l} \frac{\partial C_{1l}}{\partial y} \Big|_{y=h} \quad (6.15)$$

For component 2:

$$\frac{h^2}{2\mu_l} \frac{dP_l}{dx} \left[\left(\frac{y}{h} \right)^2 - \left(\frac{y}{h} \right) \right] \frac{\partial C_{2l}}{\partial x} = D_{2l} \frac{\partial^2 C_{2l}}{\partial y^2} \quad (6.16)$$

Inlet condition:

$$x = 0, C_{2l} = 0 \quad (6.17)$$

Boundary conditions:

$$y = 0, D_{2l} \frac{\partial C_{2l}}{\partial y} \Big|_{y=0} = \frac{Per_2}{\delta} \left(\frac{C_{2l}(x,0)RT}{H_2} - P_{out} z_2 \right) \quad (6.18)$$

$$y = h, -\frac{Q_g}{H_2} \frac{dC_{2l}}{dx} \Big|_{y=h} = wD_{2l} \frac{\partial C_{2l}}{\partial y} \Big|_{y=h} \quad (6.19)$$

6.2 Numerical Solution

It can be seen that z_1 and z_2 appear in the lower boundary conditions respectively, which makes the two partial differential equations coupled and therefore must be solved simultaneously. First we give an initial guess to z_1 and z_2 ; then, this system of partial differential equations can be solved using the Crank-Nicholson technique discussed in Chapter 4. Based on C_{1l} and C_{2l} in the solutions, Henry's law, and the following formula:

$$\bar{C}_{1l} = \frac{\int_0^h u(y)C_{1l} w dy}{Q_l} \quad (6.20)$$

$$\bar{C}_{2l} = \frac{\int_0^h u(y)C_{2l} w dy}{Q_l} \quad (6.21)$$

we can get z_1, z_2, N_g by solving formula 6.9, 6.10 and 6.11. z_1 and z_2 are compared with the initial guesses, and if either of the absolute value of the differences is bigger than the error tolerance, the new z_1 and z_2 will be substituted into the partial differential

equation system and a set of new C_{1i} and C_{2i} will be obtained. This guess-and-trial will be repeated till the error tolerance is met. Combing this trial-and trial with the Matlab code used in Chapter 4, the two-component absorption model can be solved.

Here we assume both CO_2 and H_2S inlet concentrations are 0.2017 kgmol/m^3 (i.e. 10% vol). The other parameters are the same as those in previous chapter (See Table 6.1). Polytrimethylsilylpropyne membrane was chosen as the second membrane. However, the H_2S permeability to polytrimethylsilylpropyne membrane used in the model is an estimated value as it cannot be found in literatures. Based on the fact that typically the H_2S permeability is about 2.5 to 3 times as much as CO_2 permeability in several other nonporous membranes, it was assumed H_2S permeability in this polymer is 2.5 times CO_2 permeability. This assumption is acceptable at this point in that this research is just a conceptual study rather than an engineering design. How we deduce the Henry's constants of CO_2 and H_2S in Methanol and the diffusivity of H_2S in Methanol is explained in Appendix A.

Table 6. 1 Parameters used in calculations for multi-component system

Parameter	Value
Channel height (m)	0.001
Dimension of membrane (m ²)	0.165 × 0.165
Solvent (Methanol) flow rate (10 ⁻⁸ m ³ /s)	7.12
Mixture gas flow rate (10 ⁻⁷ m ³ /s)	6.25
CO ₂ inlet concentration (kgmol/m ³)	0.2017 (10% vol)
Henry's constant (CO ₂ in Methanol)	3.89 (Henry's law: $C_{ig}H_i = C_{il}$)
Henry's constant (H ₂ S in Methanol)	18.29
Diffusivity of CO ₂ in Methanol (10 ⁻⁹ m ² /s)	8.37
Diffusivity of H ₂ S in Methanol (10 ⁻⁹ m ² /s)	3.78
Pressure of mixture gas (10 ⁶ PaA)	5.0
Temperature (K)	298.15
CO ₂ permeability (barrer)	33100
H ₂ S permeability (barrer)	82750
Pressure (permeate side) (10 ⁵ PaA)	2.0

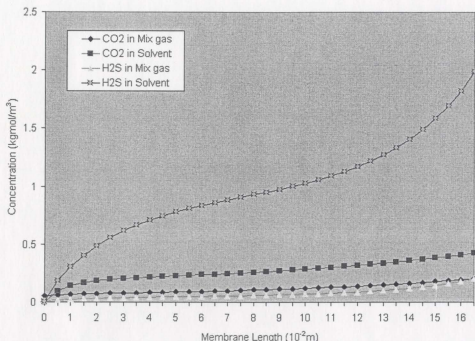


Figure 6. 2 CO₂ and H₂S concentration profiles for multi-component system

Based on the model, the CO₂ concentration in mixture gas decreases from 0.2017 to 0.0554 kgmol/m³; the average CO₂ concentration in methanol increases from 0 to 0.4245 kgmol/m³. The H₂S concentration in mixture gas decreases from 0.2017 to 0.0137 kgmol/m³; the average H₂S concentration in methanol increases from 0 to 1.9881 kgmol/m³. From Table 6.2 we can see methanol can remove H₂S more efficiently than CO₂ because of its higher Henry's constant.

Table 6. 2 Outlet CO₂ and H₂S concentrations for multi-component system for the dual-membrane contactor ($P_{out} = 2.0 \times 10^5$ PaA)

CO ₂ and H ₂ S concentration	C _{in, CO2} C _{in, H2S} (kgmol/m ³)	C _{out, CO2} (kgmol/m ³)	C _{out, H2S} (kgmol/m ³)
Mixture gas	0.2017	0.0554	0.0137
Solvent	0	0.4245	1.9881

Next we will compare the novel dual-membrane contactor with the ordinary single-membrane contactor to check if the novel dual-membrane contactor improves the performance over the ordinary membrane contactor. From Table 6.3, the outlet CO₂ concentration is lowered from 0.1139 in the ordinary single-membrane contactor to 0.0554 kgmol/m³ in the dual-membrane contactor. This means the novel configuration does improve the CO₂ removal efficiency. However, as discussed in previous chapter, because the Henry's constant of H₂S in methanol is significantly larger than that of CO₂, the outlet H₂S concentration from novel dual-membrane configuration is 0.0137 kgmol/m³, higher than 0.001, the concentration from the ordinary single-membrane configuration, that is, the dual-membrane configuration actually put a negative effect on the H₂S removal efficiency because of the large Henry's constant.

Table 6. 3 Outlet CO₂ and H₂S concentrations in mixture gas for dual-membrane and single-membrane contactors ($P_{out} = 2.0 \times 10^5$ PaA)

CO ₂ and H ₂ S concentration	C _{in, CO2} C _{in, H2S} (kgmol/m ³)	C _{out, CO2} (kgmol/m ³)	C _{out, H2S} (kgmol/m ³)
Novel contactor	0.2017	0.0554	0.0137
Ordinary Contactor	0.2017	0.1139	0.001

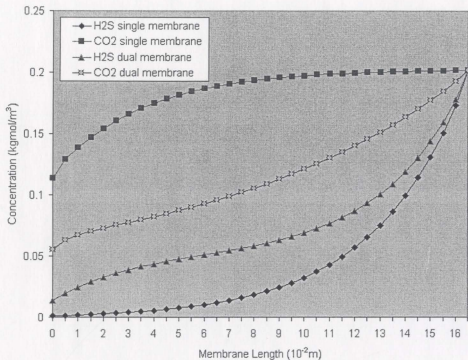


Figure 6.3 CO₂ and H₂S concentration in mixture gas profiles for dual-membrane and single-membrane contactors ($P_{out} = 2.0 \times 10^5$ PaA)

To avoid the adverse effect the high Henry's constant causes, we reduce the permeate side pressure to near zero, eliminating the partial pressure of H₂S on the permeate side, so that no reverse direction of mass transfer occurs. From Table 6.4 we can see dual-membrane configuration can lower the outlet CO₂ concentration from 0.114 to 0.038 kgmol/m³ and lower the outlet H₂S concentration from 0.001 to 0.0006 kgmol/m³. Thereby, the dual-membrane configuration can effectively improve the acid gas removal efficiency of ordinary single-membrane contactor regardless of Henry's constant when applying vacuum on the permeate side.

Table 6.4 Outlet CO₂ and H₂S concentrations in mixture gas for dual-membrane and single-membrane contactors ($P_{out} = 0$ PaA)

CO ₂ and H ₂ S concentration	C_{in, CO_2} C_{in, H_2S} (kgmol/m ³)	C_{out, CO_2} (kgmol/m ³)	C_{out, H_2S} (kgmol/m ³)
Novel contactor	0.2017	0.0377	0.0006
Ordinary Contactor	0.2017	0.1139	0.001

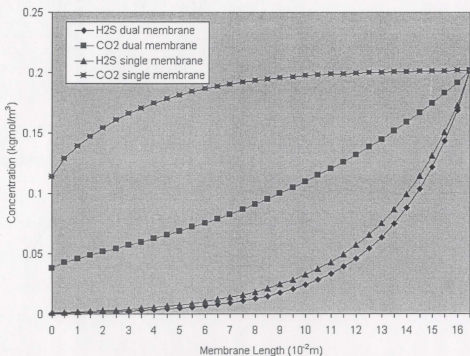


Figure 6.4 CO₂ and H₂S concentration profiles from dual-membrane and single-membrane contactors ($P_{out} = 0$)

Chapter 7

Conclusions

7.1 Summary

This thesis conceptually proposes two dual-membrane configurations to improve the performance of the ordinary single-membrane contactor. In Configuration 1, a second porous membrane is added and a flow of sweeping gas is introduced on the permeate side of the second membrane; in Configuration 2, the second membrane is a nonporous one, and a low pressure (slightly higher than atmosphere pressure) is applied on the permeate side of the nonporous membrane. Theoretically both configurations can partially regenerate the solvent stream simultaneously with the absorption process, thereby obtaining a better efficiency. To verify the proposals and check how the new configurations can improve the performance, we modeled the new configurations and ordinary single-membrane contactor with partial differential equations and solved them numerically based on single-component absorption. A series of analysis was implemented based on the solutions to check how various parameters affect the acid gas removal performance. Finally, because configuration 2 is more practical from an engineering perspective, and pure single-component absorption actually is rare in engineering application, the mathematical model of configuration 2 and corresponding numerical technique are expanded to suit multi-component absorption.

7.2 Conclusion

Based on the analysis and the comparison between new dual-membrane configuration and ordinary single-membrane contactor, it can be concluded that:

1. Both novel dual-membrane configurations can substantially improve the acid gas removal efficiency of ordinary single-membrane contactor under suitable parameter choice and operating conditions;
2. For both configurations, the counter current flow pattern can result in a better acid gas removal efficiency compared to the co-current flow pattern;
3. From the engineering perspective, configuration 2 is more practical than configuration 1 to improve the performance of ordinary membrane contactor;
4. The channel height poses a significant impact on the performance of Configuration 2; the smaller the channel height, the better removal performance can be expected.
5. The permeate side pressure is a very important parameter; the smaller the permeate side pressure, the better removal performance for Configuration 2 can be expected. When the permeate side pressure is too large, the second membrane will impose a negative effect on the gas removal efficiency.
6. Only when Henry's constant is in a certain range, Configuration 2 can improve the efficiency of the ordinary membrane contactor. When Henry's constant is too large, the second membrane will impose a negative effect on the gas removal efficiency.
7. The greater the diffusivity, the more efficiency improvement can be expected from the dual-membrane contactor relative to the ordinary membrane contactor.
8. The large solvent flow rate is helpful for the absorption efficiency for both ordinary and novel membrane contactors. Only when the solvent flow rate is in a certain range,

the dual membrane system can show a significant effect on improving the removal efficiency.

9. The larger the permeability, the better removal performance can be expected. However, when permeability is larger than a certain value, increasing permeability will not result in a significant improvement to the performance.
10. The larger the mixture gas pressure, the better removal efficiency can be expected from the novel dual membrane contactor.

7.3 Follow-up work

All the analysis and predictions regarding the novel dual-membrane contactors are based on mathematical models and therefore at a conceptual stage, to verify whether and how the configurations can improve the performance realistically, an experiment should be designed and carried out in the following work. In addition, issues such as concentration polarization are difficult to incorporate into the model as the particular membranes have not been specified. Once membranes have been selected the concentration polarization effects can be quantified through experimentation and correlations and incorporated into the model. The study should be extended to hollow fibre modules in the next step of the work in that hollow fibre modules bear more advantages over the plate-and-frame modules.

References

1. P. S. Kumar, 2002. *Development and Design of Membrane Gas Absorption Processes*, Ph. D. Thesis, University of Twente, The Netherlands.
2. Marcel Mulder, 1996. *Basic Principles of Membrane Technology*, Springer, The Netherlands.
3. A. Malek, K. Li, and W. K. Teo, 1997. "Modeling of Microporous Hollow Fiber Membrane Modules Operated under Partially Wetted Conditions", *Industrial & Engineering Chemistry Research*, Vol. 36, pp. 784-793.
4. S. Karoor and K. K. Sirkar, 1993. "Gas Absorption Studies in Microporous Hollow Fiber Membrane Modules", *Industrial & Engineering Chemistry Research*, Vol. 32, pp. 674-684.
5. M. Mavroudi, S. P. Kaldis, G. P. Sakellariopoulou, 2003. "Reduction of CO₂ emissions by a membrane contacting process", *Fuel*, Vol. 82, pp. 2153-2159.
6. R. W. Fox and A. T. McDonald, 1998. *Introduction to Fluid Mechanics*, 5th edition, John Wiley & Sons Inc, New York.
7. K. A. Hoff et al, 2003. "Modelling of Membrane Reactor", *International Journal of Chemical Reactor Engineering*, Vol.1, Article A9.
8. R. Byron Bird, Warren E. Stewart and Edwin N. Lightfoot, 2002. *Transport Phenomena*, 2nd Edition, John Wiley & Sons Inc, New York.
9. A. H. P. Skelland, 1974. *Diffusional Mass Transfer*, John Wiley & Sons Inc, New York.
10. Terrence J. Akai, 1993. *Applied Numerical Methods for Engineers*, John Wiley & Sons Inc, New York.

11. W. Ji, S. K. Sikdar, S. Hwang, 1994. "Modeling of Multicomponent Pervaporation for Removal of Volatile Organic Compounds from Water", *Journal of Membrane Science*, Vol. 93, pp. 1-19.
12. H. Yeh, 2003. "Solvent Extraction in Double-Flow Parallel-Plate Membrane Modules", *J. Chin. Inst. Chem. Engrs*, Vol. 34, pp. 635-642
13. John H. Mathews, Kurtis D. Fink, 2004. *Numerical Methods: Using Matlab*, 4th Edition, Prentice-Hall Pub. Inc., New Jersey.
14. J. W. Thomas, *Numerical Partial Differential Equations: Finite Difference Methods*, Springer, New York.
15. Robert C. Reid, John M. Prausnitz, Bruce E. Poling, 1987. *The Properties of Gases and Liquids*, 4th edition, McGraw-Hill, New York.
16. K. Fischer, J. Chen, M. Petri, J. Gmehling, 2002. "Solubility of H₂S and CO₂ in N-Octyl-Pyrrolidone and H₂S in Methanol and Benzene", *AIChE Journal*, Vol. 48, pp. 887-893.
17. Y. S. Won, D. K. Chung, and A. F. Mills, 1981. "Density, Viscosity, Surface Tension, and Carbon Dioxide Solubility and Diffusivity of Methanol, Ethanol, Aqueous Propanol, and Aqueous Ethylene Glycol at 25 °C", *J. Chem. Eng. Data*, Vol. 26, pp. 140-141.

Appendix A

The Properties of H₂S and CO₂ in Methanol

A.1 Diffusion Coefficient of H₂S in Methanol

Because no diffusion coefficient of H₂S in methanol can be found in literature, Nakanishi correlation is used to estimate it as follows [15].

$$D_{AB} = \left[\frac{9.97 \times 10^{-8}}{(I_A V_A)^{1/3}} + \frac{2.40 \times 10^{-8} A_B S_B V_B}{I_A S_A V_A} \right] \frac{T}{\eta_B} \quad (\text{A.1})$$

where D_{AB} denotes the diffusion coefficient of solute A in solvent B , cm²/s, V_A and V_B are liquid molar volumes at 298.15 K, cm³/mol, I_A , S_A , S_B , and A_B are Nakanishi parameters given in the literature, and η_B is the solvent viscosity, in cP. When ϵ solute is not a liquid at 298.15 K, the following correlation could be used to obtain the V_A ...

$$V_A(298.15\text{K}) = 1.065V_A(T_b) \quad (\text{A.2})$$

where T_b denotes the normal boiling point, and $V_A(T_b)$ can be obtained by:

$$V_A(T_b) = 0.285V_c^{1.048} \quad (\text{A.3})$$

where V_c is critical volume, 98.6 cm³/mol for H₂S. Based on formula A.3 and A.4, we have $V_A(298.15\text{K}) = 37.31$ cm³/mol. In addition, $V_B = 40.47$ cm³/mol, $\eta_B = 0.547$ cP,

$I_A = 1.25$, $S_A = 1$, $A_B = 2.0$, $S_B = 1$ and $T = 298.15$ K. Substituting all the parameters into equation A.1, we have $D_{AB} = 3.78 \times 10^{-9}$ m²/s.

A.2 Henry's Constant of H₂S in Methanol

In some literatures, Henry's law is expressed as:

$$P_i = H_i' x_i \quad (\text{A.4})$$

where x_i denotes mole fraction of component i in liquid, P_i denotes the partial pressure in gas phase, Pa, and H_i' denotes the Henry's constant, Pa. The Henry's constant used in the thesis is based on:

$$C_{ig} H_i = C_{il} \quad (\text{A.5})$$

where the unit of C_{ig} and C_{il} is the mole concentration, kgmol/m³. Submitting equation A.4 into gas state equation:

$$C_{ig} = \frac{n_i}{V} = \frac{P_i}{RT} \quad (\text{A.6})$$

we have

$$C_{ig} = \frac{H_i'(C_{il}/C_f)}{RT} = \frac{H_i'}{C_f RT} C_{il} \quad (\text{A.7})$$

where C_f denotes the total mole concentration of solution, kgmol/m³, and can be treated as pure solvent due to the dilute solution assumption.

Thereby,

$$H_i = \frac{C_f RT}{H_i'} \quad (\text{A.8})$$

For H_2S , $H' = 3.35 \times 10^6$ Pa, we have $H = 18.29$ [16].

A.3 Diffusion Coefficient of CO_2 in Methanol

From the literature, the diffusion coefficient of CO_2 in methanol is 8.37×10^{-9} m^2/s [17].

A.4 Solubility of CO_2 in Methanol

From the literature, the solubility of CO_2 in methanol is 1.57×10^{-6} $\text{kgmol}/\text{m}^3\text{Pa}$ [17].

$$C_{it} = 0.159P_i = 0.159C_{ig}RT \quad (\text{A.9})$$

Based on Formula A.5, we have $H = 3.89$.

Appendix B

Crank-Nicholson Technique

The Crank-Nicholson method is a very efficient technique for parabolic equations. To demonstrate the methodology of the Crank-Nicholson method, the following partial differential equation in terms of time and coordinates x is taken as a prototype.

$$u_t(x,t) = c^2 u_{xx}(x,t), \quad 0 \leq x \leq a, \quad 0 \leq t \leq b \quad (\text{B.1})$$

Initial condition:

$$u(x,0) = f(x), \quad 0 \leq x \leq a \quad (\text{B.2})$$

Boundary conditions:

$$u(0,t) = g_1(t) = c_1, \quad 0 \leq t \leq b \quad (\text{B.3})$$

$$u(a,t) = g_2(t) = c_2, \quad 0 \leq t \leq b \quad (\text{B.4})$$

This particular problem can be solved analytically; however, for the purpose of illustration, it will be solved numerically as follows. The first step is to discretize the domain by placing a grid over the domain. As shown in Figure B.1, the grid spacing Δx is equal to $\frac{a}{n-1}$, denoted as h , and Δt is equal to $\frac{b}{m-1}$, denoted as k . Now the space-time domain of the problem is approximated by the lattice of points. The solution to the problem can be approximated at the points on the lattice.

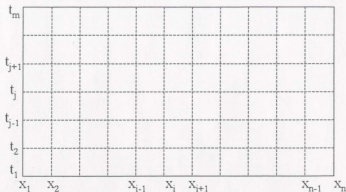


Figure B. 1 Grid on time-space domain

Derived from central-difference method, u_t can be approximated by the following equations at the point $(x, t + \frac{k}{2})$ (See Figure B.2).

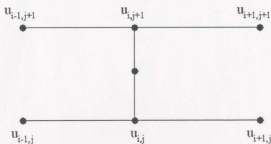


Figure B. 2 Crank-Nicholson method

$$u_t(x, t + \frac{k}{2}) = \frac{u(x, t + k) - u(x, t)}{k} + O(k^2) \quad (\text{B.5})$$

The approximation for u_{xx} at the point $(x, t + \frac{k}{2})$ is obtained by averaging the approximation values of $u_{xx}(x, t)$ and $u_{xx}(x, t + k)$, with the error within $O(h^2)$.

$$u_{xx}(x, t) = \frac{u(x-h, t) - 2u(x, t) + u(x+h, t)}{h^2} + O(h^2) \quad (\text{B.6})$$

Thereby,

$$u_{xx}(x, t + \frac{k}{2}) = \frac{1}{2}(u_{xx}(x, t) + u_{xx}(x, t + k)) \quad (\text{B.7})$$

That is

$$\begin{aligned} u_{xx}(x, t + \frac{k}{2}) &= \frac{1}{2h^2}(u(x-h, t+k) - 2u(x, t+k) + u(x+h, t+k)) \\ &+ u(x-h, t) - 2u(x, t) + u(x+h, t) + O(h^2) \end{aligned} \quad (\text{B.8})$$

By substituting $u_i(x, t + \frac{k}{2})$ and $u_{xx}(x, t + \frac{k}{2})$ into the prototype equation, neglecting $O(h^2)$ and $O(k^2)$, and letting $u_{i,j}$ stand for $u(x_i, t_j)$, the following equation can be reached:

$$\frac{u_{i,j+1} - u_{i,j}}{k} = c^2 \frac{u_{i-1,j+1} - 2u_{i,j+1} + u_{i+1,j+1} + u_{i-1,j} - 2u_{i,j} + u_{i+1,j}}{2h^2} \quad (\text{B.9})$$

To implement the Crank-Nicholson method, the formula is rearranged in the form:

$$-\lambda u_{i-1,j+1} + (2 + 2\lambda)u_{i,j+1} - \lambda u_{i+1,j+1} = (2 - 2\lambda)u_{i,j} + \lambda(u_{i-1,j} + u_{i+1,j}) \quad (\text{B.10})$$

where

$$\lambda = c^2 k / h^2 \quad (\text{B.11})$$

Now all terms on the right hand of the equation are known, and $u_{i-1,j+1}$, $u_{i,j+1}$ and $u_{i+1,j+1}$ on the left hand are unknown. The matrix formulation corresponding this equation for the prototype problem is

condition, $u_{n,2}$ values can be calculated from the matrix equation. By proceeding forward in positive t direction, all values on the lattice can be obtained.

A slight variation that is often encountered is the nonhomogeneous equation, for example,

$$F(x,t)u_t(x,t) = c^2 u_{xx}(x,t) \quad (\text{B.17})$$

For this kind of partial differential equation, we only need to substitute

$$F((i-1)h, (j-1.5)k) \quad (\text{B.18})$$

and finite difference formulas of u_t and u_{xx} at the point $(x, t + \frac{k}{2})$ into Formula B.17 in order to write a logical difference scheme. Then this equation can be solved numerically [14].

Appendix C

Matlab and Maple Codes

C.1 Matlab code

C.1.1 Configuration 1 and ordinary membrane contactor under co-current conditions

```
%% Variables
%% l denotes the length and the width of the membrane, micron;
%% h denotes the distances between two membranes, micron;
%% c denotes the inlet CO2 concentration of mixture gas, mol/cubic micron;
%% d1 denotes the CO2 diffusivity in liquid, square micron/s;
%% vg1 and vg3 denote the flow rate of the sweeping gas and the mixture
%% gas, respectively, cubic micron/s;
%% v12 denotes the flow rate of the solvent, cubic micron/s;
%% hen denotes the Henry's constant;
%% li denotes the length increment and hi denotes the height increment,
%% micron;
%% P denotes the pressure of mixture gas, Pa;
%% T denotes the temperature of system, K.
```

```
l=165000;
h=1000;
c=0.00000000000000004034;
d1=8370;
vg1=156250000000;
v12=71200000000;
vg3=625000000000;
hen=3.89;
li=33;
hi=100;
P=5000000;
T=298.15;
```

```
m=l/li;
n=h/hi+1;
```

```
%% CONSTRUCT MATRIX FORMULA AB*A=B
```

```
A=zeros(m,n);
A(1,1)=0.0;
A(1,2:n-1)=0.0;
A(1,n)=c*hen;
```

```
%% CONSTRUCT MATRIX AB
AB=zeros(n,n);
```

```
AB(1,1:2)=[1+vg1*hi/(li*d1*hen*li),-1];
```

```
for j=2:n-1
```

```
AB(j,j-1:j+1)=[-(d1/(2*hi^2)*li*h*li)/(6*vl2),2*(d1/(2*hi^2)*li*h*li)/  
(6*vl2)+0.25-(((j-1)*hi-h/2)^2)/h^2,-(d1/(2*hi^2)*li*h*li)/(6*vl2)];  
end
```

```
AB(n,n-1:n)=[1/hi,vg3/(l*d1*hen*li)-1/hij];
```

```
%% CALCULATE MATRIX A, CO2 CONCENTRATION IN THE SOLVENT PHASE
```

```
for i=2:m
```

```
%% CONSTRUCT MATRIX B
```

```
B=zeros(n,1);
```

```
B(1,1)=vg1*hi/(li*d1*hen*li)*A(i-1,1);
```

```
for j=2:n-1
```

```
B(j,1)=(d1/(2*hi^2)*li*h*li)/(6*vl2)*A(i-1,j-1)-(2*(d1/(2*hi^2)  
*li*h*li)/(6*vl2)-(0.25-(((j-1)*hi-h/2)^2)/h^2))*A(i-1,j)  
+(d1/(2*hi^2)*li*h*li)/(6*vl2)*A(i-1,j+1);
```

```
end
```

```
B(n,1)=vg3/(l*d1*hen*li)*A(i-1,n);
```

```
%% OBTAIN MATRIX A USING SUBROUTINE "kufact"
```

```
A(i,1:n)=feval("kufact",AB,B);
```

```
end
```

```
%% GENERATE CONCENTRATION PROFILES IN MIX GAS, LIQUID, AND SWEEPING GAS
```

```
Pro=zeros(m,3); %% mole concentration profiles in three phases
```

```
Percentage=zeros(m,2); %% CO2 content in mixture and sweeping gas phases
```

```
for i=1:m
```

```
Pro(i,1)=A(i,1)/hen*1E15; %%sweeping gas
```

```
Percentage(i,1)=(A(i,1)/hen*1E15)/(P*0.001/(8.3145*T));
```

```
Pro(i,3)=A(i,n)/hen*1E15; %%mixture gas
```

```
Percentage(i,2)=(A(i,n)/hen*1E15)/(P*0.001/(8.3145*T));
```

```
end
```

```
%% OBTAIN THE AVERAGE MOLE CONCENTRATION IN SOLVENT
```

```
for i=1:m
```

```
Sum=0;
```

```
for j=1:n-1
```

```
Sum=((((j-1)*hi/h-((j-1)*hi/h)^2)+(j*hi/h-(j*hi/h)^2))/2*(A(i,j)  
+A(i,j+1)))/2+Sum;
```

```
end
```

```
Ave=6/(n-1)*Sum;
```

```
Pro(i,2)=Ave*1E15;
```

```
Ave=0;
```

```
end
```

```
%% TAKE VALUES AT POINT 0,0.5,1,1.5... 16.5CM
```

```
G=zeros(34,3);
```

```
CP=zeros(34,2);
```

```
G(1,1:3)=Pro(1,1:3);
```

```
CP(1,1:2)=Percentage(1,1:2);
```

```
for i=2:33
```

```
G(i,1:3)=Pro(1+151*(i-1),1:3);
```

```
CP(i,1:2)=Percentage(1+151*(i-1),1:2);
end
```

```
G(34,1:3)=Pro(m,1:3);
CP(34,1:2)=Percentage(m,1:2);
```

```
inlet=A(1,n)/hen
outlet=A(m,n)/hen
```

C.1.2 Configuration 1 and ordinary membrane contactor under counter current conditions

%% Variables

```
%% l denotes the length and the width of the membrane, micron;
%% h denotes the distances between two membranes, micron;
%% c denotes the inlet CO2 concentration of mixture gas, mol/cubic micron;
%% d1 denotes the CO2 diffusivity in liquid, square micron/s;
%% vg1 and vg3 denote the flow rate of the sweeping gas and the mixture
%% gas, respectively, cubic micron/s;
%% vl2 denotes the flow rate of the solvent, cubic micron/s;
%% hen denotes the Henry's constant;
%% li denotes the length increment and hi denotes the high increment,
%% micron;
%% P denotes the pressure of mixture gas, Pa;
%% T denotes the temperature of system, K;
%% er denotes error.
```

```
l=165000;
h=1000;
c=0.00000000000000004034;
d1=8370;
vg1=156250000000;
vg2=71200000000;
vg3=625000000000;
hen=3.89;
li=33;
hi=100;
er=0.00000000000000000001;
P=5000000;
T=298.15;
```

```
m=l/li;
n=h/hi+1;
```

```
%% CONSTRUCT MATRIX FORMULA AB*A=B
```

```
A=zeros(m,n);
A(1,1)=0.0;
A(1,2:n-1)=0.0;
A(1,n)=0.0;
```

```
%% CONSTRUCT MATRIX AB
AB=zeros(n,n);
```

```

AB(1,1:2)=[1+vg1*hi/(li*d1*hen*I),-1];
for j=2:n-1
    AB(j,j+1)=[-(d1/(2*hi^2)*li*h*I)/(6*vl2),2*(d1/(2*hi^2)*li*h*I)/
        (6*vl2)+0.25-(((j-1)*hi-h/2)^2)/h^2,-(d1/(2*hi^2)*li*h*I)/(6*vl2)];
end

AB(n,n-1:n)=[1/hi,vg3/(I*d1*hen*Ii)-1/hI];

%% CALCULATE MATRIX A, CO2 CONCENTRATION IN THE SOLVENT PHASE
a=0;
b=c*hen;
iteration=0;
while abs(A(m,n)/hen-c)>er
    A(1,n)=(a+b)/2;

    for i=2:m
        %% CONSTRUCT MATRIX B
        B=zeros(n,1);
        B(1,1)=vg1*hi/(li*d1*hen*I)*A(i-1,1);
        for j=2:n-1
            B(j,1)=(d1/(2*hi^2)*li*h*I)/(6*vl2)*A(i-1,j-1)-(2*(d1/(2*hi^2)*li*h*I)/
                (6*vl2)-(0.25-(((j-1)*hi-h/2)^2)/h^2))*A(i-1,j)+(d1/(2*hi^2)*li*h*I)/(6*vl2)*A(i-1,j+1);
        end
        B(n,1)=vg3/(I*d1*hen*Ii)*A(i-1,n);
        %% OBTAIN MATRIX A USING SUBROUTINE "kufact"
        A(i,1:n)=feval('kufact',AB,B);
    end

    number=A(m,n)/hen-c;

    if number>0
        b=A(1,n);
    elseif number<0
        a=A(1,n);
    else number=0
        break;
    end

    iteration=iteration+1;
end

%% GENERATE CONCENTRATION PROFILES IN MIX GAS, LIQUID, AND SWEEPING GAS
Pro=zeros(m,3);%% mole concentration profiles in three phases
Percentage=zeros(m,2); %% CO2 content in mixture and sweeping gas phases

for i=1:m
    Pro(i,1)=A(i,1)/hen*1E15;%% sweeping gas
    Percentage(i,1)=(A(i,1)/hen*1E15)/(P*0.001/(8.3145*T));
    Pro(i,3)=A(i,n)/hen*1E15;%% mixture gas
    Percentage(i,2)=(A(i,n)/hen*1E15)/(P*0.001/(8.3145*T));
end
%% OBTAIN THE AVERAGE MOLE CONCENTRATION IN SOLVENT
for i=1:m

```

```

Sum=0;
for j=1:n-1
    Sum=((j-1)*hi/h-((j-1)*hi/h)^2)+(j*hi/h-(j*hi/h)^2)/2*(A(i,j)+A(i,j+1))/2+Sum;
end
Ave=6/(n-1)*Sum;
Pro(i,2)=Ave*1E15;
Ave=0;
end

outlet=A(1,n)/hen
inlet=A(m,n)/hen

%%% TAKE VALUES AT POINT 0,0.5,1,1.5... 16.5CM
G=zeros(34,3);
CP=zeros(34,2);
G(1,1:3)=Pro(1,1:3);
CP(1,1:2)=Percentage(1,1:2);

for i=2:33
    G(i,1:3)=Pro(1+151*(i-1),1:3);
    CP(i,1:2)=Percentage(1+151*(i-1),1:2);
end

G(34,1:3)=Pro(m,1:3);
CP(34,1:2)=Percentage(m,1:2);

```

C.1.3 Configuration 2 under co-current conditions

```

%%% Variables
%%% l denotes the length and the width of the membrane, micron;
%%% h denotes the distances between two membranes, micron;
%%% c denotes the inlet CO2 concentration of mixture gas, mol/cubic micron;
%%% d1 denotes the CO2 diffusivity in liquid, square micron/s;
%%% Per denotes the CO2 permeability of the nonporous membrane,
%%% mol*micron/(square micron*s*Pa);
%%% thick denotes the thickness of the nonporous membrane, micron;
%%% Pout denotes the permeate side pressure, Pa;
%%% vg3 denote the flow rate of the mixture gas, cubic micron/s;
%%% vi2 denotes the flow rate of the solvent, cubic micron/s;
%%% hen denotes the Henry's constant;
%%% li denotes the length increment and hi denotes the height increment,
%%% micron;
%%% R denotes the gas constant, Pa*cubic micron/(mol*K);
%%% P denotes the pressure of mixture gas, Pa;
%%% T denotes the temperature of system, K.

```

```

l=165000;
h=1000;
c=0.00000000000000004034;
d1=8370;
Per=1062.5E-20;
thick=50;
Pout=200000;

```

```

vl2=7120000000;
vg3=-625000000000;
hen=3.89;
li=33;
hi=100;
R=8.3145*1000000000000000000;
T=298.15;
P=5000000;

```

```

m=li;
n=h/hi+1;

```

```

%% CONSTRUCT MATRIX FORMULA AB*A=B

```

```

A=zeros(m,n);
A(1,1)=0.0;
A(1,2:n-1)=0.0;
A(1,n)=c*hen;

```

```

%% CONSTRUCT MATRIX AB

```

```

AB=zeros(n,n);

```

```

AB(1,1:2)=[d1/hi+Per*R*T/(thick*hen),-d1/hi];

```

```

for j=2:n-1

```

```

AB(j,j-1:j+1)=[-(d1/(2*hi^2)*li*h^1)/(6*vl2),2*(d1/(2*hi^2)*li*h^1)/
(6*vl2)+0.25-(((j-1)*hi-h/2)^2)/h^2,-(d1/(2*hi^2)*li*h^1)/(6*vl2)];
end

```

```

AB(n,n-1:n)=[1/hi,vg3/(l*d1*hen*li)-1/hi];

```

```

%% CALCULATE MATRIX A, CO2 CONCENTRATION IN THE SOLVENT PHASE

```

```

for i=2:m

```

```

%% CONSTRUCT MATRIX B

```

```

B=zeros(n,1);

```

```

B(1,1)=Per*Pout/thick;

```

```

for j=2:n-1

```

```

B(j,1)=(d1/(2*hi^2)*li*h^1)/(6*vl2)*A(i-1,j-1)-(2*(d1/(2*hi^2)*li*h^1)/
(6*vl2)-(0.25-(((j-1)*hi-h/2)^2)/h^2))*A(i-1,j)+(d1/(2*hi^2)*li*h^1)/(6*vl2)*A(i-1,j+1);

```

```

end

```

```

B(n,1)=vg3/(l*d1*hen*li)*A(i-1,n);

```

```

%% OBTAIN MATRIX A USING SUBROUTINE "kufact"

```

```

A(i,1:n)=feval('kufact',AB,B);

```

```

end

```

```

%% GENERATE THE CONCENTRATION PROFILES IN MIXTURE GAS, LIQUID

```

```

Pro=zeros(m,2);%% mole concentration profiles in two phases

```

```

Percentage=zeros(m,1); %% CO2 content in mixture gas phase

```

```

for i=1:m

```

```

Pro(i,1)=A(i,n)/hen*1E15;

```

```

Percentage(i,1)=(A(i,n)/hen*1E15)/(P*0.001/(8.3145*T));

```

```

end

```

```

%% OBTAIN THE AVERAGE MOLE CONCENTRATION IN SOLVENT

```

```

for i=1:m
    Sum=0;
    for j=1:n-1
        Sum=((j-1)*hi/h-((j-1)*hi/h)^2)+(j*hi/h-(j*hi/h)^2))/2*(A(i,j)+A(i,j+1))/2+Sum;
    end
    Ave=6/(n-1)*Sum;
    Pro(i,2)=Ave*1E15;
    Ave=0;
end

inlet=A(1,n)/hen
outlet=A(m,n)/hen

%% TAKE VALUES AT POINT 0,0.5,1,1.5... 16.5CM
G=zeros(34,2);
CP=zeros(34,1);
G(1,1:2)=Pro(1,1:2);
CP(1,1)=Percentage(1,1);
for i=2:33
    G(i,1:2)=Pro(1+151*(i-1),1:2);
    CP(i,1)=Percentage(1+151*(i-1),1);
end

G(34,1:2)=Pro(m,1:2);
CP(34,1)=Percentage(m,1);

```

C.1.4 Configuration 2 under counter current conditions

```

%% Variables
%% l denotes the length and the width of the membrane, micron;
%% h denotes the distances between two membranes, micron;
%% c denotes the inlet CO2 concentration of mixture gas, mol/cubic micron;
%% d1 denotes the CO2 diffusivity in liquid, square micron/s;
%% Per denotes the CO2 permeability of the nonporous membrane,
%% mol*micron/(square micron*s*Pa);
%% thick denotes the thickness of the nonporous membrane, micron;
%% Pout denotes the permeate side pressure, Pa;
%% vg3 denote the flow rate of the mixture gas, cubic micron/s;
%% vl2 denotes the flow rate of the solvent, cubic micron/s;
%% hen denotes the Henry's constant;
%% li denotes the length increament and hi denotes the hight increment,
%% micron;
%% R denotes the gas constant,Pa*cubic micron/(mol*K);
%% P denotes the pressure of mixture gas, Pa;
%% T denotes the temperature of system, K;
%% er denotes the error.

```

```

l=165000;
h=1000;
c=0.00000000000000004034;
P=5000000;
d1=8370;
Per=1062.5E-20;

```

```

thick=50;
Pout=200000;
vl2=71200000000;
vg3=625000000000;
hen=3.89;
li=33;
hi=100;
er=0.00000000000000000001;
R=8.3145*1000000000000000000;
T=298.15;

```

```

m=l/li;
n=h/hi+1;

```

```

%% CONSTRUCT MATRIX FORMULA AB*A=B

```

```

A=zeros(m,n);
A(1,1)=0.0;
A(1,2:n-1)=0.0;
A(1,n)=0.0;

```

```

%% CONSTRUCT MATRIX AB

```

```

AB=zeros(n,n);

```

```

AB(1,1:2)=[d1/hi+Per*R*T/(thick*hen),-d1/hi];

```

```

for j=2:n-1

```

```

AB(j,j-1:j+1)=[-(d1/(2*hi^2)*li*h^1)/(6*vl2),2*(d1/(2*hi^2)*li*h^1)/
(6*vl2)+0.25-(((j-1)*hi-h/2)^2)/h^2,-(d1/(2*hi^2)*li*h^1)/(6*vl2)];
end

```

```

AB(n,n-1:n)=[1/hi,vg3/(l*d1*hen*li)-1/hi];

```

```

%% CALCULATE MATRIX A, CO2 CONCENTRATION IN THE SOLVENT PHASE

```

```

a=0;
b=c*hen;
iteration=0;
while abs(A(m,n)/hen-c)>er
A(1,n)=(a+b)/2;

```

```

for i=2:m

```

```

%% CONSTRUCT MATRIX B

```

```

B=zeros(n,1);

```

```

B(1,1)=Per*Pout/thick;

```

```

for j=2:n-1

```

```

B(j,1)=(d1/(2*hi^2)*li*h^1)/(6*vl2)*A(i-1,j-1)-(2*(d1/(2*hi^2)*li*h^1)/
(6*vl2)-(0.25-(((j-1)*hi-h/2)^2)/h^2))*A(i-1,j)+(d1/(2*hi^2)*li*h^1)/(6*vl2)*A(i-1,j+1);
end

```

```

B(n,1)=vg3/(l*d1*hen*li)*A(i-1,n);

```

```

%% OBTAIN MATRIX A USING SUBROUTINE "kufact"

```

```

A(i,1:n)=feval("kufact",AB,B);

```

```

end

```

```

number=A(m,n)/hen-c;

if number>0
b=A(1,n);
elseif number<0
a=A(1,n);
else number=0
break;
end
iteration=iteration+1;
end

%% GENERATE THE CONCENTRATION PROFILES IN MIXTURE GAS AND LIQUID
Pro=zeros(m,2);
Percentage=zeros(m,1);
for i=1:m
Pro(i,1)=A(i,n)/hen*1E15;
Percentage(i,1)=(A(i,n)/hen*1E15)/(P*0.001/(8.3145*T));
end
%% OBTAIN THE AVERAGE MOLE CONCENTRATION IN SOLVENT
for i=1:m
Sum=0;
for j=1:n-1
Sum=((j-1)*hi/h-((j-1)*hi/h)^2)+(j*hi/h-(j*hi/h)^2))/2*(A(i,j)+A(i,j+1))/2+Sum;
end
Ave=6/(n-1)*Sum;
Pro(i,2)=Ave*1E15;
Ave=0;
end

outlet=A(1,n)/hen
inlet=A(m,n)/hen

%% TAKE VALUES AT POINT 0,0.5,1,1.5... 16.5CM
G=zeros(34,2);
CP=zeros(34,1);
G(1,1:2)=Pro(1,1:2);
CP(1,1)=Percentage(1,1);
for i=2:33
G(i,1:2)=Pro(1+151*(i-1),1:2);
CP(i,1)=Percentage(1+151*(i-1),1);
end

G(34,1:2)=Pro(m,1:2);
CP(34,1)=Percentage(m,1);

```

C.1.5 Multi-component system under counter current conditions

```

%% Variables
%% l denotes the length and the width of the membrane, micron;
%% h denotes the distances between two membranes, micron;
%% c denotes the inlet CO2 concentration of mixture gas, mol/cubic micron;
%% cB denotes the inlet H2S concentration of mixture gas, mol/cubic micron;
%% d1 denotes the CO2 diffusivity in liquid, square micron/s;

```

%% d1B denotes the H2S diffusivity in liquid, square micron/s;
 %% Per denotes the CO2 permeability of the nonporous membrane,
 %% mol*micron/(square micron*s*Pa);
 %% PerB denotes the H2S permeability of the nonporous membrane,
 %% thick denotes the thickness of the nonporous membrane, micron;
 %% Pout denotes the permeate side pressure, Pa;
 %% vg3 denote the flow rate of the mixture gas, cubic micron/s;
 %% vl2 denotes the flow rate of the solvent, cubic micron/s;
 %% hen denotes the Henry's constant of CO2 in liquid;
 %% hen denotes the Henry's constant of H2S in liquid;
 %% li denotes the length increment and hi denotes the hight increment, micron;
 %% R denotes the gas constant, Pa*cubic micron/(mol*K);
 %% P denotes the pressure of mixture gas, Pa;
 %% T denotes the temperature of system, K;
 %% er denotes the error.

l=165000;
 h=1000;
 c=0.00000000000000002017;
 cB=0.00000000000000002017;
 d1B=8370;
 d1B=3780;
 Per=1062.5E-20;
 PerB=2656.3E-20;
 thick=50;
 Pout=200000;
 vl2=71200000000;
 vg3=625000000000;
 hen=3.89;
 henB=18.29;
 li=33;
 hi=100;
 er=0.0000000000000000001;
 R=8.3145*1000000000000000000;
 T=298.15;
 P=5000000;

delta=0.000000000000001;
 epsilon=0.00000000000001;
 max1=100;
 error=0.00001;

m=l/li;
 n=h/hi+1;

%% CONSTRUCT MATRIX FORMULA AB*A=B

A=zeros(m,2*n);
 A(1,1)=0.0;
 A(1,2:n-1)=0.0;
 A(1,n)=0;
 A(1,n+1)=0.0;
 A(1,n+2:2*n-1)=0.0;
 A(1,2*n)=0;

%% CONSTRUCT MATRIX AB

```

AB=zeros(2*n,2*n);
%% FOR COMPONENT CO2
AB(1,1:2)=[d1/hi+Per*R*T/(thick*hen),-d1/hi];

for j=2:n-1
    AB(j,j-1:j+1)=[-(d1/(2*hi^2)*li*h^1)/(6*vl2),2*(d1/(2*hi^2)*li*h^1)/(6*vl2)+0.25-(((j-1)*hi-
h/2)^2)/h^2,-(d1/(2*hi^2)*li*h^1)/(6*vl2)];
end

AB(n,n-1:n)=[1/hi,-vg3/(l*d1*hen*li)-1/hi];

%%FOR COMPONENT H2S
AB(n+1,n+1:n+2)=[d1B/hi+PerB*R*T/(thick*henB),-d1B/hi];

for j=n+2:2*n-1
    AB(j,j-1:j+1)=[-(d1B/(2*hi^2)*li*h^1)/(6*vl2),2*(d1B/(2*hi^2)*li*h^1)/(6*vl2)+0.25-(((j-1)*hi-
h/2)^2)/h^2,-(d1B/(2*hi^2)*li*h^1)/(6*vl2)];
end

AB(2*n,2*n-1:2*n)=[1/hi,-vg3/(l*d1B*henB*li)-1/hi];

%% MATRIX AB IS FINISHED

%% CALCULATE MATRIX A, CO2 AND H2S CONCENTRATION IN THE SOLVENT PHASE
a=0;
b=c*hen;
iteration=0;
while abs(A(m,n)/hen-c)>er
    A=zeros(m,2*n);
    A(1,n)=(a+b)/2;
    ANN=A(1,n)

    aB=0;
    bB=cB*henB;
while abs(A(m,2*n)/henB-cB)>er

    A(1,2*n)=(aB+bB)/2;
    A2NN=A(1,2*n)

for i=2:m
    YA=0.5;
    YB=0.5;
    P1=[625000000000,0.2,0.8];

while abs(YA-P1(2))>error

    YA=P1(2);
    YB=P1(3);
%%CONSTRUCT MATRIX B

B=zeros(2*n,1);

%% FOR COMPONENT CO2
B(1,1)=Per*Pout/thick*YA;

for j=2:n-1

```

```

    B(j,1)=(d1/(2*hi^2)*li*h^i)/(6*vl2)*A(i-1,j-1)-(2*(d1/(2*hi^2)*li*h^i)/(6*vl2)-(0.25-(((j-1)*hi-
    h/2)^2)/h^2))*A(i-1,j)+(d1/(2*hi^2)*li*h^i)/(6*vl2)*A(i-1,j+1);
end
B(n,1)=-vg3/(l*d1*hen*li)*A(i-1,n);

%% FOR COMPONENT H2S
B(n+1,1)=PerB*Pout/thick*YB;
for j=n+2:2*n-1
    B(j,1)=(d1B/(2*hi^2)*li*h^i)/(6*vl2)*A(i-1,j-1)-(2*(d1B/(2*hi^2)*li*h^i)/(6*vl2)-(0.25-(((j-n-1)*hi-
    h/2)^2)/h^2))*A(i-1,j)+(d1B/(2*hi^2)*li*h^i)/(6*vl2)*A(i-1,j+1);
end
B(2*n,1)=-vg3/(l*d1B*henB*li)*A(i-1,2*n);

%%MATRIX B IS FINISHED

%% OBTAIN MATRIX A USING SUBROUTINE "kufact"
A(i,1:2*n)=feval('kufact',AB,B);

Sum=0;
SumB=0;
for j=1:n-1
    Sum=((j-1)*hi/h-((j-1)*hi/h)^2)+(j*hi/h-(j*hi/h)^2))/2*(A(i,j)+A(i,j+1))/2+Sum;
    SumB=((j-1)*hi/h-((j-1)*hi/h)^2)+(j*hi/h-(j*hi/h)^2))/2*(A(i,j+n)+A(i,j+n+1))/2+SumB;
end
Ave=6/(n-1)*Sum;
AveB=6/(n-1)*SumB;

[P1,iter,err]=feval('newdim','F','JF',P1,delta,epsilon,max1,vg3,A(i,n),vl2,Ave,c,A(i,2*n),AveB,cB);

    end
end

ww=A(m,2*n)/henB
SS=A(m,n)/hen

numberB=A(m,2*n)/henB-cB;

if numberB>0
    bB=A(1,2*n);
elseif numberB<0
    aB=A(1,2*n);
else numberB=0
    break;
end

iteration=iteration+1
end

GAA=A(m,2*n)/henB
GBB=A(m,n)/hen

number=A(m,n)/hen-c;

if number>0
    b=A(1,n);
elseif number<0

```

```

a=A(1,n);
else number=0
break;
end

```

```
end
```

```
%% GENERATE THE CONCENTRATION PROFILES IN MIXTURE GAS AND LIQUID
```

```
Pro=zeros(m,4);
Percentage=zeros(m,2);
```

```
for i=1:m
Pro(i,1)=A(i,n)/hen*1E15;
Percentage(i,1)=(A(i,n)/hen*1E15)/(P*0.001/(8.3145*T));
Pro(i,3)=A(i,2*n)/henB*1E15;
Percentage(i,2)=(A(i,2*n)/henB*1E15)/(P*0.001/(8.3145*T));
end
```

```
for i=1:m
Sum=0;
SumB=0;
for j=1:n-1
Sum=((j-1)*hi/h-((j-1)*hi/h)^2)+(j*hi/h-(j*hi/h)^2))/2*(A(i,j)+A(i,j+1))/2+Sum;
SumB=((j-1)*hi/h-((j-1)*hi/h)^2)+(j*hi/h-(j*hi/h)^2))/2*(A(i,j+n)+A(i,j+n+1))/2+SumB;
end
Ave=6/(n-1)*Sum;
AveB=6/(n-1)*SumB;
Pro(i,2)=Ave*1E15;
Pro(i,4)=AveB*1E15;
Ave=0;
AveB=0;
end
```

```
%% TAKE VALUES AT POINT 0,0.5,1,1.5... 16.5CM
```

```
G=zeros(34,4);
CP=zeros(34,2);
G(1,1:4)=Pro(1,1:4);
CP(1,1:2)=Percentage(1,1:2);
for i=2:33
G(i,1:4)=Pro(1+151*(i-1),1:4);
CP(i,1:2)=Percentage(1+151*(i-1),1:2);
end
```

```
G(34,1:4)=Pro(m,1:4);
CP(34,1:2)=Percentage(m,1:2);
```

C.2 Maple code

C.2.1 Configuration 1

```
> Eqg1:=0.625*D(CAg1)(x)=0.0009446*16.5*(3.89*CAg1(x)-CAL(x));
```

```
Eqg1 := 0.625 D(CAg1)(x) = 0.0606291510 CAg1(x) - 0.01558590 CAL(x)
```

>Eq1:=0.0712*D(CAL)(x)=0.0009446*16.5*(3.89*CAg1(x)-CAL(x))-
0.0009446*16.5*(CAL(x)-3.89*CAg2(x));

$$\text{Eq1} := 0.0712 D(\text{CAL})(x) = 0.0606291510 \text{ CAg1}(x) - 0.03117180 \text{ CAL}(x) \\ + 0.0606291510 \text{ CAg2}(x)$$

>Eqg2:=0.15625*D(CAg2)(x)=0.0009446*16.5*(CAL(x)-3.89*CAg2(x));

$$\text{Eqg2} := 0.15625 D(\text{CAg2})(x) = 0.01558590 \text{ CAL}(x) - 0.0606291510 \text{ CAg2}(x)$$

> sys:=Eqg1,Eq1,Eqg2;

$$\text{sys} := 0.625 D(\text{CAg1})(x) = 0.0606291510 \text{ CAg1}(x) - 0.01558590 \text{ CAL}(x),$$

$$0.0712 D(\text{CAL})(x) = 0.0606291510 \text{ CAg1}(x) - 0.03117180 \text{ CAL}(x)$$

$$+ 0.0606291510 \text{ CAg2}(x),$$

$$0.15625 D(\text{CAg2})(x) = 0.01558590 \text{ CAL}(x) - 0.0606291510 \text{ CAg2}(x)$$

> initial:=CAg1(16.5)=0.0004034,CAL(0)=0,CAg2(0)=0;

$$\text{initial} := \text{CAg1}(16.5) = 0.0004034, \text{CAL}(0) = 0, \text{CAg2}(0) = 0$$

> evalf(dsolve({sys,initial},{CAg1(x),CAL(x),CAg2(x)}));

$$\{\text{CAL}(x) = 0.002487097369 - 0.002374970195 \exp(-0.03771308907 x)$$

$$- 0.0001121271729 \exp(-0.6911130155 x),$$

$$\text{CAg2}(x) = -0.0006762591858 \exp(-0.03771308907 x) + 0.0006393566501$$

$$+ 0.00003690253595 \exp(-0.6911130155 x),$$

$$\text{CAg1}(x) = -0.0004396214010 \exp(-0.03771308907 x) + 0.0006393566501$$

$$- 0.000003547893553 \exp(-0.6911130155 x)\}$$

C.2.2 Configuration 2

> Eqg:=0.625*D(CAg)(x)=0.0009446*16.5*(3.89*CAg(x)-CAL(x));

$$\text{Eqg} := 0.625 D(\text{CAg})(x) = 0.0606291510 \text{ CAg}(x) - 0.01558590 \text{ CAL}(x)$$

>Eq1:=0.0712*D(CAL)(x)=0.0009446*16.5*(3.89*CAg(x)-CAL(x))-

1.3856*0.000000000001*16.5*(8.3145*298.15*CAL(x)*1000000/3.89-200000);

$$\text{Eq1} := 0.0712 D(\text{CAL})(x) = 0.0606291510 \text{ CAg}(x) - 0.03015535039 \text{ CAL}(x)$$

$$+ 0.000004572480000$$

> sys:=Eqg,Eq1;

$$\text{sys} := 0.625 D(\text{CAg})(x) = 0.0606291510 \text{ CAg}(x) - 0.01558590 \text{ CAL}(x),$$

$$0.0712 D(\text{CAL})(x) = 0.0606291510 \text{ CAg}(x) - 0.03015535039 \text{ CAL}(x)$$

+ 0.000004572480000

```
> initial:=CAg(16.5)=0.0004034,CAI(0)=0;
  initial := CAg(16.5) = 0.0004034, CAI(0) = 0
> evalf(dsolve({sys},{CAg(x),CAI(x)}));
{CAI(x) = exp(0.05238746694 x) _C2 + exp(-0.3789110274 x) _C1
  + 0.0003138402532,
  CAg(x) = 0.5588951433 exp(0.05238746694 x) _C2 + 0.00008067872834
  + 0.0523986429 exp(-0.3789110274 x) _C1}
> eqg:=0.0004034=.5588951433*exp(.5238746694e-1*16.5)*_C2+.8067872834e-
4+.523986429e-1*exp(-.3789110274*16.5)*_C1;
  eqg := 0.0004034 = 1.326574163 _C2 + 0.00008067872834 + 0.0001009478472 _C1
> eql:=0=exp(.5238746694e-1*0)*_C2+exp(-.3789110274*0)*_C1+.3138402532e-3;
  eql := 0 = 1. _C2 + 1. _C1 + 0.0003138402532
> solve({eqg,eql},{_C1,_C2});
  {_C1 = -0.0005571568535, _C2 = 0.0002433166003}
> CAg(x)=.5588951433*exp(.5238746694e-1*x)*.2433166003e-3+.8067872834e-
4+.523986429e-1*exp(-.3789110274*x)*(-.5571568535e-3);
  CAg(x) = 0.0001359884662 exp(0.05238746694 x) + 0.00008067872834
  - 0.00002919426301 exp(-0.3789110274 x)
> CAI(x)=exp(.5238746694e-1*x)*.2433166003e-3+exp(-.3789110274*x)*(-
.5571568535e-3)+.3138402532e-3;
  CAI(x) = 0.0002433166003 exp(0.05238746694 x)
  - 0.0005571568535 exp(-0.3789110274 x) + 0.0003138402532
```

C.2.3 Ordinary membrane contactor

```
> Eqg:=0.625*D(CAg)(x)=0.0009446*16.5*(3.89*CAg(x)-CAI(x));
  Eqg := 0.625 D(CAg)(x) = 0.0606291510 CAg(x) - 0.01558590 CAI(x)
> Eql:=0.0712*D(CAI)(x)=0.0009446*16.5*(3.89*CAg(x)-CAI(x));
  Eql := 0.0712 D(CAI)(x) = 0.0606291510 CAg(x) - 0.01558590 CAI(x)
> sys:=Eqg,Eql;
  sys := 0.625 D(CAg)(x) = 0.0606291510 CAg(x) - 0.01558590 CAI(x),
```

$$0.0712 D(CAl)(x) = 0.0606291510 CAg(x) - 0.01558590 CAl(x)$$

> initial:=CAg(16.5)=0.0004034,CAI(0)=0;

initial := CAg(16.5) = 0.0004034, CAI(0) = 0

> evalf(dsolve({sys,initial},{CAg(x),CAI(x)}));

{CAg(x) = 0.0004288297274 - 0.0001900353791 exp(-0.1218964483 x),

CAI(x) = -0.001668147639 exp(-0.1218964483 x) + 0.001668147639}

